Dissertation zur Erlangung des Doktorgrades

der Fakultät für Chemie und Pharmazie

der Ludwig-Maximilians-Universität München

Identification of the novel antitumor targets of Lagunamide A and Neocarzilin A

Yudong Hu

aus

Zhoukou, Henan, China

2023

Erklärung

Diese Dissertation wurde im Sinne von § 7 der Promotionsordnung vom 28. November 2011 von Frau Prof. Dr. Angelika M. Vollmar betreut.

Eidesstattliche Versicherung

Diese Dissertation wurde eigenständig und ohne unerlaubte Hilfe erarbeitet.

München, den 01. Juni 2023

_____

(Yudong Hu)

Dissertation eingereicht am:	13.06.2023
1. Gutachterin:	Prof. Dr. Angelika M. Vollmar
2. Gutachter:	Prof. Dr. Stefan Zahler
Mündliche Prüfung am:	17.07.2023

To my family

Contents

ABSTRACT

1. Abstract

Natural products are a rich source of bioactive compounds and have traditionally contributed to the discovery and exploration of prospective drug development targets. Novel targets, particularly for cancer, are desperately needed to study cancer biology and develop precision therapeutics. Inspired by the promising anticancer activities of the marine cyanobacterial product Lagunamide A (Lag A) and the streptomyces carzinostaticusin product Neocarzilin A (NCA), we performed in depth studies on their modes of action.

For Lagunamide A, a biologically active natural compound, the cellular target is yet unidentified. With an affinity-based approach (ABPP), we failed to identify a target protein. In contrast, by using thermal proteome profiling, we found three proteins EYA3, SMC1A and NDC80 as putative targets. For validation of the proposed targets, genetic depletion of EYA3 showed only limited impact on antagonizing the anti-proliferative and pro-apoptotic effect of Lag A. However, EYA3 turned out to be important for DNA damage repair since incubation with Lag A sensitized cancer cells to doxorubicin treatment. Thus, this work not only shows that Lag A might serve as a chemosensitizing agent in the tumor context, but also pinpoints that depending on the target proteins, different target identification techniques are required.

Besides the chemoresistance machinery, cell proliferation is another hotspot in the field of cancer research. Our previous study showed that the natural compound NCA exhibited potent anti-migratory and anti-proliferative effects on cancer cells. We have previously identified VAT-1 as a putative anti-migratory target of NCA. However, the target and mechanism for the anti-proliferative effect of NCA were unknown to date. Affinity-based protein profiling (ABPP) based on an NCA-derived probe, and subsequent mass spectrometry were employed to identify additional potential target proteins of NCA. For validation of the proposed targets, we used genetic knockdown (with siRNA) or knockout (with CRISPR/Cas9) and over-expression approaches. By applying ABPP, Bone Marrow Stromal Antigen 2 (BST-2) was identified as it was highly enriched by binding to an NCA-derived probe. Binding of BST-2 to the probe

was outcompeted by NCA itself, proposing BST-2 as a target of NCA. Silencing or knockout of BST-2 decreased the anti-proliferative action of NCA against HeLa cells, while overexpression or reconstitution of BST-2 increased sensitivity of cells towards NCA, thereby supporting the hypothesis of BST-2 as an anti-proliferative target of NCA. In-depth mechanistic studies revealed that NCA promoted BST-2 degradation via the lysosomal pathway and influenced the EGFR signaling pathway via disturbing lipid rafts, which in turn regulated cell proliferation. In conclusion, we identify BST-2 as an innovative target of NCA, and NCA as an interesting lead structure for inhibiting cancer cell proliferation.

INTRODUCTION

2. Introduction

2.1 Cancer and Therapy

2.1.1 Cancer statistics

Cancer is a major public health problem and ranks as a leading cause of death worldwide[1]. According to GLOBOCAN data, an estimated 19.3 million new cancer cases (18.1 million excluding nonmelanoma skin cancer) and over 10.0 million cancer-related deaths (9.9 million excluding nonmelanoma skin cancer) occurred worldwide in 2020[2], primarily due to both aging and growth of the population as well as changes in the prevalence and distribution of the main risk factors for cancer[3]. Notably, the coronavirus disease 2019 (COVID-19) pandemic delayed cancer diagnosis and treatment due to health care facility closures, disruptions in employment and health insurance, and fear of COVID-19 exposure. The delays in diagnosis and treatment may lead to an uptick in advanced‐stage disease and mortality, but it still needs several years to reflect the overall effect[4].

2.1.2 Treatment options for cancer

'Hallmarks of Cancer' reviews by Hanahan and Weinberg reduced the complexities of cancer as a disease into key traits: sustaining proliferative signaling, evading growth suppressors, resisting cell death, enabling replicative immortality, inducing angiogenesis and activating invasion and metastasis. Advances in the past decade have added four biological processes, including genome instability and mutation reprogramming of energy metabolism, evading immune destruction and tumor-promoting inflammation[5] (Figure 1). Amongst them, the most fundamental feature of cancer cells is their capacity to sustain persistent proliferation. However, the particular identities and origins of the proliferative signals working inside normal tissues were poorly understood two decades ago and in general remain so. Despite its side-effects, systemic chemotherapy targeting cancer cell proliferation remains the major of choice[6]. In addition, the notion of 'Hallmarks of cancer' is a potent guide for

translational research focused on enhancing and developing cancer diagnosis, screening, therapies, and life quality of patients[7]. Remarkably, the challenge will be to integrate all of this information to understand the key determinants of particular carcinogenesis pathways, to identify new therapeutic targets, and to identify modes of adaptive resistance to therapy. Cancer therapy still suffers from a limited range of molecular targets that can be addressed by small molecules, although huge efforts have been made to identify suitable targets to improve the treatment of cancer in recent decades[8]. This emphasizes the need of identifying and validating novel and druggable targets to provide new choices for cancer therapy. Besides, drug resistance remains a significant barrier to attaining cures in cancer patients, while combination chemotherapy established a new paradigm for cancer therapy, leading to the creation of increasingly complicated regimens to overcome drug resistance[9]. In these contexts, natural products are used as valuable research tools to identify the molecular cancer targets for cell proliferation or drug resistance.

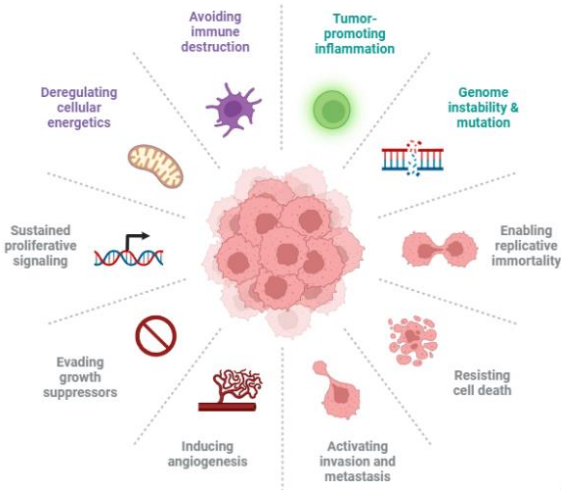

Figure 1: The Hallmarks of cancer. The graphical figure was adapted from Hanahan and Weinberg[5].

2.2 Natural products

Throughout the ages, natural products provide not only the basic needs for daily life, but also supply pharmaceuticals for the treatment of a wide range of diseases, including cancer. Natural products or their structural relatives account for approximately 50% of cancer chemotherapeutic drugs. In addition, it is anticipated that between 1981 and 2019, natural products accounted for around 25% of all newly

authorized anti-cancer drugs[10, 11], including microbes, plants, and marine sources. For example, the first plant-derived drugs to be used in clinical practice were vinblastine (VLB) and vincristine (VCR), which were used to treat diabetes in several Asian countries, were extracted from the plant *Catharanthus roseus* (also known as *Vinca rosea* or the *rosey periwinkle*). Besides, an undoubtedly successful star is Taxol (paclitaxel) which shows potent efficacy against refractory breast and ovarian cancers. It is obtained from the bark of the *Pacific yew Taxus brevifolia* and is the bestselling anticancer drug at present[12]. In addition to botanical medications, marine natural products are another major source of anti-cancer therapeutic leads. 10,000 new structures have been separated from the marine since the mid-1960s. Trabectedin is the first marine-isolated anti-tumor drug, which was approved for the treatment of advanced soft tissue sarcoma, was isolated from the Caribbean tunicate Ecteinascidia turbinate.

The main challenges for natural products studies are the acquisition of sufficient quantity of compounds, identification of the major active compounds and the knowledge of natural product molecular mechanisms. Firstly, shortage of compound supply often occurred to natural products, such as taxol, it took 20 years from its discovery in 1967 until the first clinical responses with ovarian cancer in 1987, and now the issue was resolved by a commercially feasible semi-synthetic procedure from 10-deacetylbaccatin III; Secondly, for the discovery of effective compounds, High-throughput screening may lead to identify the effective pro-drug structure and has become a standard method for drug discovery in the pharmaceutical industry. Thirdly, current research is still struggling to identify the targets or modes of action of natural compounds. To solve this problem, some new cutting-edge technologies are being developed. For instance, cellular thermal shift assay or thermal proteome profiling[13] which do not need chemical modification, and competitive chemoproteomic profiling based on Affinity-based protein profiling (ABPP) that is used to map proteome-wide targets. Both are currently employed to investigate the direct targets of natural compounds.

2.2.1 Lagunamide A

Microorganisms (prokaryotes and eukaryotes) play an important role and are versatile producers in the development of natural product chemistry and medicinal treatment. The most common producers of prokaryotes are unicellular bacteria, specifically *Bacillus* and *Pseudomonas* species, filamentous actinomycetes, myxobacteria, and cyanobacteria[14]. Marine cyanobacteria have emerged as a valuable source in producing structurally diverse bioactive natural products[15], which exhibit a range of physiological functions, such as antimicrobial, antimalarial, cytotoxic, and neurotoxic properties[16, 17]. This makes marine cyanobacterial compounds an attractive source of therapeutic agents for cancer therapy.

Lagunamide A (Lag A) and its analogues lagunamides B and C are potent cyclic depsipeptides isolated from marine cyanobacterium *Lyngbya majuscula*, a sponge collected in Pulau Hantu Besar of Singapore[18]. Lag A (Figure 2) belongs to a class of structurally related marine natural products, such as aurilides, which have potent anticancer effects due to their cytotoxic activities[19, 20]. Previous studies described potent growth inhibitory activities of lagunamides in the low nanomolar range against a panel of cancer cell lines[21, 22], including murine leukemia cell P388, lung cancer cells A549, melanoma cells A375, stomach cancer cells BGC-823. Furthermore, first biochemical studies of Lag A revealed that the cytotoxic effect of the natural compound was triggered via mitochondria-mediated apoptosis[23]. Interestingly, also for aurilide, a mitochondrial phenotype has been described in tumor cell lines, and the mitochondrial protein prohibitin has been proposed as molecular target in an affinity-based approach[19]. However, target identification studies for Lag A are still lacking. Given the need for novel targets in cancer therapy, strategies to unravel the mode of action of potent natural products are of major importance.

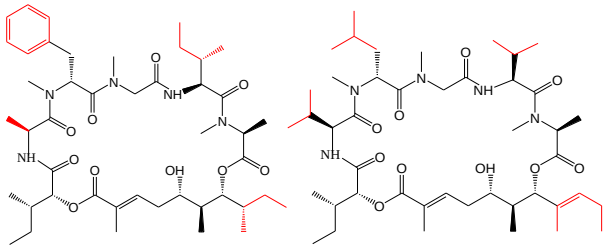

Figure 2. Structures of Lagunamide A and Aurilide. The red color labelled in the structures are the different parts of Aurilide from Lag A.

2.2.2 Neocarzilin A

Besides cyanobacteria, actinomycetes are other important sources for natural products. Actinomycetales species produce over 10,000 bioactive compounds, amongst them, 7600 from Streptomyces and 2500 from rare actinomycetes species—representing the largest category (45%) of bioactive microbial metabolites. Neocarzilin A (NCA) and Neocarzilin B (NCB) were initially isolated from the actinomycete Streptomyces carzinostaticus var. F41. by Nozoe et al. in 1992 (Figure 3). Meanwhile, they showed that NCA exhibited a potent cytotoxic activity against K562 chronic myelogenous leukemia cells with IC_{50} of 0.06 µg/ml. Until now, no structure-activity relationship (SAR) studies of Neocarzilins in human cancer cells have been published. However, the acidic hydroxyl group appears to be important for biological activity of NCA, as the corresponding methylether demonstrated only moderate cytotoxic activity with an IC_{50} of 2 µg/ml. Furthermore, previous work in our lab indicated that NCA inhibited cell proliferation and cell migration significantly and in terms of target discovery with chemical proteomics, it was found that NCA affected cell migration via binding to the synaptic vesicle membrane protein VAT-1[24]. However, we found that VAT-1 knock-out had no significant influence on the anti-proliferative effect of NCA. Thus, the potential anti-proliferative targets of NCA remain unclear.

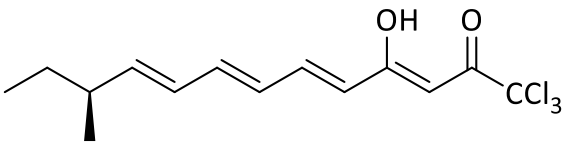

Figure 3. Structure of Neocarzilin A.

2.3 EYA3

2.3.1 Origin of EYA3 and function

Eyes absent homolog 3 (EYA3) belongs to the eyes absent family proteins, which were initially discovered as factors to maintain normal eye development and are essential regulators of embryonic development. The mutations of EYA proteins cause developmental defects of diverse tissues such as ear, kidney[25], heart[26], muscle[27], thymus and lung[28].

There are four EYA family members (EYA1–4) in mammals and their function is closely related with their unique structure. All of them contain 2 domains important for their function: a highly conserved C-terminal EYA domain (ED) and a less conserved N-terminal transactivation domain (NTD). The ED mediates the protein tyrosine phosphatase (PTP) activity that has been implicated in regulating cell proliferation and apoptosis[25, 29, 30], migration[31, 32], invasion[31], and angiogenesis[33]. While the NTD has EYA transcriptional co-activator function and contains the Ser/Thr phosphatase activity that has been implicated in innate immunity[34, 35].

It is of note that the well-established function of EYA proteins are as transcriptional cofactors to the Six family of homeoproteins[36, 37]. When EYA proteins bind to Six family members, which actively contributes to the translocation of EYAs from the cytoplasm to the nucleus[36-38]. Although EYA proteins have no recognized DNA binding activity, EYA/Six complex acts as transcriptional co-activators via a transactivation domain[37, 39, 40]. Thus, the complex influences the transcription of c-Myc[41], cyclin D[42], VEGF-C[43], and TGF-β[44].

2.3.2 The role of EYA3 in cancer: status quo

EYA gene mutations have long been linked to human developmental problems, including branchio-oto-renal (BOR) syndrome, oto-facio-cervical (OFC) syndrome[45], Cardio facial syndrome[46], Congenital cataract[47]. On the other hand, expression or over-expression of EYA family members have been reported in Ewing sarcoma[48],

colorectal[49], ovarian[50], breast cancers[29, 31], malignant peripheral nerve sheath tumors[51] and Wilms tumors[52]. Furthermore, over-expression of EYA family members has been correlated with poor prognosis of cancer.

Lingdi Zhang discovered that EYA3 modulated c-Myc stability and tumor growth through regulating PP2A activity[53]. Yuhua Wang revealed that both EYA3 deletion and pharmacologic reduction of EYA3 tyrosine phosphatase activity in Ewing sarcoma cells inhibited tumor growth and angiogenesis[54]. In addition, EYAs played a role in tumor growth and metastasis in breast cancer, mostly via their interaction with Six1[55]. All of the research on EYA proteins proposed that they are novel therapeutic and druggable targets. Novel chemicals or well-established compounds are now being investigated to inhibit or influence the activity of EYA proteins, among them benzbromarone and benzarone are the most thoroughly validated EYA PTP inhibitors[56].

2.3.3 EYA3 and DNA damage repair

Despite the fact that EYA proteins have a unique structure that includes both phosphor-tyrosine and phospho-serine/threonine residues, until now only few substrates were validated, including Histone H2A.X (phosphotyrosine-pY-142)[57], estrogen receptor β (pY36)[30] and WD repeat-containing protein 1 (WDR1)[58]. Amongst them, researchers were particularly interested in the Histone protein H2AX because of its relevance in the DNA damage and repair process.

As known, genome integrity is a hallmark of cancer and the repair of double-strand breaks caused by either endogenous (cellular metabolism) or exogenous (environmental factors, such as ionizing radiation (IR), ultraviolet (UV) radiation, and various chemical agents) sources is critical for genome integrity maintenance. Tumors with specific DNA repair defects can be completely dependent on back-up DNA repair pathways for their survival. Thus, the deregulation of DNA repair pathways is associated with the initiation and progression of cancer. Upon DNA damage, histone variant H2AX is rapidly phosphorylated at serine 139 site, which is referred to DNA

damage repair foci called γH2AX to facilitate the recruitment of damage response proteins. So far, the change of γH2AX was considered as a marker to monitor DNA damage and repair process. Recently, phosphorylation of H2AX at tyrosine 142 has been discovered. Xiao et al. demonstrated that H2AX was constitutively phosphorylated at tyrosine 142 and that when DNA was damaged, Y142 phosphorylation level decreased while Ser139 phosphorylation level increased[59]. In addition, Peter J. Cook et al showed that the EYA proteins dephosphorylated H2AX at Y142 and dephosphorylation of Y142 was necessary for the assembly of the formation of functional DNA-damage repair complexes and cell survival[57, 60]. Therefore, the EYA proteins are being extensively researched as potential targets for cancer therapies.

2.4 BST-2

2.4.1 Origin of BST-2 and function

BST-2, also known as CD317, HM1.24 or tetherin, originally named bone marrow stromal cell antigen 2, was cloned in 1995 from a rheumatoid arthritis derived synovial cell line[61]. BST-2 is an IFN-inducible type II transmembrane protein mainly at the surface of cells and within several endosomal membrane compartments, including the trans-Golgi network (TGN) as well as early and recycling endosomes[62-64]. BST-2 contains an N-terminus cytoplasmic tail followed by a transmembrane domain, an extracellular coiled-coiled domain and a C-terminus glycophosphatidylinositol (GPI) anchor embedded in cholesterol-enriched lipid rafts along the cell membrane[63, 65] (Figure 4). BST-2 was originally identified as a membrane protein in terminally differentiated human B cells of patients with multiple myeloma[66, 67]. In terms of function, BST-2 is known for its tethering and antiviral functions, since its overexpression tethers/retains nascent virions on the surface of infected cells and prevents infection of new target cells[68, 69], which was found in 2008 as a host cell 'restriction factor' inhibited by the HIV-1 accessory protein Vpu[68, 70]. More specially, HIV-1 escapes BST-2-mediated restriction through the function of its accessory

protein viral protein U (Vpu)[71, 72] and most studies have found that Vpu reduced cell surface levels of BST-2[73] via various mechanisms including lysosomal degradation, proteasomal degradation, and/or sequestration/retargeting of BST-2 to the trans-Golgi network (reviewed in[74]). In addition, BST-2 is thought to mediate host immune response by activating NF-κB through the YXY motif on the cytoplasmic domain of BST-2 and the interaction with transforming growth factor beta-activated kinase 1 (TAK1)[75-77].

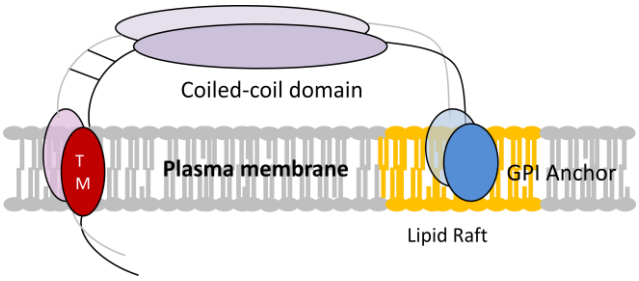

Figure 4. Structure of BST-2.

2.4.2 The role of BST-2 in cancer and cell proliferation

Although overexpression of BST-2 tethers virions on the cell membrane and negatively regulates virus replication, it is likely that BST-2 is upregulated in several cancers, including ovarian cancer[78], neoplastic B cells[66], breast cancer[79], endometrial cancer[80], gastric cancer and lung cancer[81] and elevated BST-2 expression might positively influence cancer cell behavior[79, 82-85]. There is direct evidence for a role for BST-2 in two cancers. BST-2 antibody-mediated ADCC has been demonstrated to be effective in the treatment of myeloma[86, 87]. Besides, treatment using a monoclonal antibody targeting BST-2 decreased tumor growth and increased survival in a multiple myeloma mouse mode[88]. BST-2 was directly involved in the development of breast cancer and breast cancer cells lost their capacity to proliferate *in vivo* upon BST-2 knockdown[89], although the attributes of BST-2 that orchestrate its tumorigenic behavior are not well understood. In addition, BST-2 gene knockdown decreased gastric cancer cell development, indicating that BST-2 could be a useful therapeutic target for gastric cancer[90]. Meanwhile, BST-2-mediated cancer development has

been linked to a variety of cellular mechanisms such as cell-to-cell adhesion, anchorage-independent growth, migration, and invasion[79, 89, 91].

The extracellular C-terminal GPI anchor of BST-2 enables its association with the lipid rafts[92] and these specialized membrane microdomains—which are abundant in cholesterol, sphingolipids, and certain proteins—play important roles in intracellular signaling, trafficking, and pathogen–host interactions. As such, lipid rafts facilitated interactions between signaling molecules, and their disruption (for example, by cholesterol deficiency) reduces the ability of receptors to activate[93]. BST-2 has been shown to regulate the organization of lipid rafts microdomains and related signaling[92], including the epithelial growth factor receptor (EGFR). As one of the first receptor tyrosine kinases (RTKs) to be discovered, EGFR is commonly dysregulated in malignancies[94, 95] and has received substantial research as a model for RTK-mediated signaling and a target for cancer therapy[94-96]. EGFR is associated with lipid rafts and the activation of EGFR is regulated by its localization to lipid rafts[97-99]. Guizhong Zhang revealed that the lipid raft-associated BST-2 regulated the release of EGFR from lipid rafts and the activation of EGFR. As such, BST-2 was able to dissociate EGFR from lipid rafts, enabling constitutive EGFR activation and signaling regardless of binding to its cognate ligands, including EGF, TGF[94], and AREG[100]. Thus, BST-2 activated the EGFR downstream signaling pathway of Akt and Erk 1/2, leading to the proliferation of tumor cells[101].

2.5 Aims of Study

The natural products Lagunamide A (Lag A) and Neocarzilin A (NCA) were discovered decades ago, but despite their striking activity against cancer cells, modes of action studies of these potent molecules are still missing up to date. Considering the emergence of proteomic methods for target identification, we aimed to elucidate their mechanisms of action by identifying cellular interaction partners and investigate its antitumor effects to reveal their potential as anticancer drug leads as well as molecular probes.

The precise goals of this thesis were summarized as follows:

Part I: Lagunamide A --- Mode of action studies with focus on mitochondrial function and indirect target

1. Functional characterization in tumor cells concerning proliferation and apoptosis

2. Analysis of mitochondrial function

3. Target identification via thermal protein profiling (TPP) performed by Dietrich Mostert (Group of Prof. Sieber, Department of Chemistry, Technical University of Munich, Germany)

4.Target verification and revelation of its role in cancer cells

Part II: Neocarzilin A --- Direct target and mode of action elucidation

1. Identify the cellular anti-proliferative target of NCA by proteomic Affinity-based protein profiling (ABPP) in cooperation with Josef Braun (Group of Prof. Sieber, Department of Chemistry, Technical University of Munich, Germany)

2. Validate the identified target protein via genetic knockdown, over-expression and knockout experiments

3. Elucidate the mode of action of NCA on cell proliferation

MATERIALS AND METHODS

3. Materials and Methods

3.1 Materials

3.1.1 Compounds

Lagunamide A was kindly provided by Prof. Dr. Uli Kazmaier (Institute for Organic Chemistry, Saarland University, Saarbrücken, Germany). Neocarzilin A was kindly supplied by Prof. Dr. Stephan A. Sieber (Chair of Organic Chemistry II, Technical University of Munich, Munich, Germany). Both compounds were dissolved in sterilized DMSO and stored at -20°C in small aliquots.

3.1.2 Antibodies

Table 1 List of primary and secondary antibodies

Antibodies	SOURCE	IDENTIFIER
Goat Anti-Mouse IgG1, HRP-linked	Abcam	Cat# ab97240, RRID:AB_10695944
Goat anti-rabbit IgG (H+L), HRP-linked	Jackson ImmunoResearch Labs	Cat# 111-035-144, RRID: AB_2307391
Goat anti-Rabbit IgG Alexa Fluor™ 488	Thermo Fisher	Cat# A-11008, RRID:AB_143165
Goat anti-rat IgG Alexa Fluor™ 546	Thermo Fisher Scientific	Cat# A-11081, RRID:AB_2534125
Mouse monoclonal anti- Phospho-STAT3 (Tyr705)	Cell Signaling	Cat# 9138, RRID:AB_331262
Mouse monoclonal anti-BST-2	Santa Cruz	Cat# sc-390719
Mouse monoclonal anti-EYA3	Santa Cruz	Cat# sc-515626, RRID:AB_2927642
Rabbit monoclonal Anti-EGF Receptor	Cell Signaling	Cat# 4267, RRID:AB_2895042
Rabbit monoclonal anti-Histone H2A.X	Cell Signaling	Cat# 7631, RRID:AB_10860771
Rabbit monoclonal anti-Mitofusin-1	Cell Signaling	Cat# 14739, RRID:AB_2744531
Rabbit monoclonal anti-OPA1	Cell Signaling	Cat# 80471, RRID:AB_2734117

Antibodies	SOURCE	IDENTIFIER
Rabbit monoclonal Phospho-EGF Receptor (Tyr1068)	Cell Signaling	Cat# 48576
Rabbit polyclonal anti-Bcl-2	Cell Signaling	Cat# 2872, RRID: AB_10693462
Rabbit polyclonal anti-Bcl-xl	Cell Signaling	Cat# 2762, RRID:AB_10694844
Rabbit polyclonal anti-Cytochrome c	Cell Signaling	Cat# 4272, RRID:AB_2090454
Rabbit polyclonal anti-Mcl-1	Cell Signaling	Cat# 4572, RRID:AB_2281980
Rabbit polyclonal anti-Phospho-Histone H2A.X (Ser139)	Cell Signaling	Cat# 2577, RRID:AB_2118010
Rabbit polyclonal anti-STAT3	Cell Signaling	Cat# 9132, RRID:AB_331588
Rabbit polyclonal anti-VDAC	Cell Signaling	Cat# 4866, RRID:AB_2272627
Rat monoclonal anti-EGFR	Abcam	Cat# ab231, RRID:AB_2293306

3.1.3 Chemicals and reagents

Table 2 List of chemicals

Chemicals	Supplier
16% Formaldehyde Solution, Methanol-free	Thermo Fisher, Waltham, Massachusetts, USA
2,2,2-Trichloroethanol (TCE)	Sigma Aldrich, St. Louis, MO, USA
Ammonium persulfate (APS)	Sigma Aldrich, St. Louis, MO, USA
Bovine serum albumin (BSA)	Sigma-Aldrich
Collagen G	Biochrom AG, Berlin, Germany
Complete®	Roche Diagnostics, Penzberg, Germany
Coumaric acid	Fluka, Buchs, Switzerland
Crystal violet	Carl Roth
Dimethylsulfoxide (DMSO)	Carl Roth
Dithiothreitol (DTT)	Sigma-Aldrich, Taufkirchen, Germany
Doxorubicin –hydrochlorid (DXR)	Sigma-Aldrich
Dulbecco's Modified Eagle Medium (DMEM)	PAN Biotech, Aidenbach, Germany
Fetal calf serum (FCS)	PAN Biotech, Aidenbach, Germany
FluorSave® reagent mounting medium	Merck, Darmstadt, Germany
Glycerol	Applichem, Darmstadt, Germany
H_2DCFDA	Thermo Fisher Scientific
Hoechst 33342	Sigma-Aldrich
JC-1	Enzo
Lagunamide A	This paper
Luminol	AppliChem, Darmstadt, Germany

Chemicals	Supplier
MitoTracker™ Deep Red FM	Molecular Probes
ON-TARGETplus non-targeting control siRNA	Horizon Discovery
ON-TARGETplus Human BST-2 siRNA	Horizon Discovery
ON-TARGETplus Human EYA3 siRNA	Horizon Discovery
Page Ruler™ Prestained Protein Ladder	Thermo Fisher, Waltham, MA, USA
Penicillin/Streptomycin	PAN Biotech, Aidenbach, Germany
Penicillin/Streptomycin	PAN Biotech, Aidenbach, Germany
PowerUp™ SYBR® Green Master Mix	Applied Biosystems, Waltham, MA, USA
Primers	Metabion, Planegg, Germany
Propidium iodide (PI)	Sigma Aldrich
Pyronin Y	Sigma Aldrich, St. Louis, MO, USA
Pyruvate	Merck, Darmstadt, Germany
Rotiphorese Gel 30	Carl Roth, Karlsruhe, Germany
RPMI 1640 cell culture medium	PAN Biotech, Aidenbach, Germany
Sodium orthovanadate (Na_3VO_4)	ICN, Biomedicals, Aurora, OH, USA
Sodium dodecyl sulfate (SDS)	Carl Roth, Karlsruhe, Germany
TEMED	VWR, Radnor, PA, USA
Tris Base	Sigma-Aldrich, Taufkirchen, Germany
Triton X-100	Merck, Darmstadt, Germany
Trypsin	PAN Biotech, Aidenbach, Germany
Tween 20	Sigma-Aldrich, Taufkirchen, Germany

3.1.4 Technical equipment

Table 3 List of technical equipment

Device	Producer
BEEM® capsule G360.1	Plano GmbH, Wetzlar, Germany
ChemiDoc™ Touch Imaging System	Bio-Rad, Hercules, CA, USA
FACS Canto II	BD, Franklin Lakes, NJ, USA
Ibidi Treat µ-slide 8-well	ibidi GmbH, Munich, Germany
Leica SP8 Inverted Scanning Confocal Microscope	Leica Microsystems, Wetzlar, Germany
Nanodrop® Spectrophotometer	Peqlab Biotechnology, Erlangen, Germany
Nitrocellulose membrane	Amersham Bioscience, Freiburg, Germany
Orion II microplate Luminometer	Berthold Detection Systems GmbH
PowerPac HC, Tank Blotting System	Bio-Rad, Hercules, CA, USA
Primus 25 advanced® Thermocycler	PEQLAB Biotechnologie GmbH
QuantStudio™ 3 Real-Time PCR System	Applied Biosystems, Waltham, USA
Seahorse XFe96 Analyzer	Agilent Technologies, Santa Clara, USA
SpectraFluor Plus™	Tecan, Männedorf, Switzerland
Tecan Sunrise	Tecan, Männedorf, Switzerland
Vi-Cell™ XR	Beckman Coulter, Krefeld, Germany

3.1.5 Software

Table 4 List of software

Software name	Supplier
FlowJo 7.6	Tree Star, Ashland, OR, USA
GraphPad Prism 9	GraphPad Software, San Diego, CA, USA
ImageJ	NIH, Bethesda, MD, USA
Seahorse Wave Software	Agilent Technologies, Santa Clara, CA, USA
Seahorse XF Mito StressTest Report Generator	Agilent Technologies, Santa Clara, CA, USA

3.1.6 Critical commercial assay

Table 5 List of commercial kits

Critical commercial assay	SOURCE	IDENTIFIER
CellTiter-Blue Cell Viability	Promega	Cat# G8081
CellTiter-Glo luminescent cell viability assay	Promega	Cat# G7571
Bradford assay	Carl Roth	Cat# K015.1
Seahorse XF MitoStress Test Kit	Agilent Technologies	Cat# 102601-100
Lipid rafts staining kit	Thermo Fisher Scientific	Cat# V34403
Lipofectamine™ RNAiMAX Transfection Reagent	Thermo Fisher Scientific	Cat# 13778075
RNeasy® Mini Kit (250)	Qiagen	Cat# 74106

3.2 Cell culture

3.2.1 Cell lines

HeLa (derived from a 31-year-old female) cells were obtained from the DSMZ and grown in DMEM supplemented with 10% fetal bovine serum. S-Jurkat cells which were derived from the peripheral blood of a 14-year-old boy, were kindly provided by P. H. Krammer (DKFZ, Heidelberg, Germany) and cultivated in RPMI 1640 containing 10% FBS, 100 U/ml penicillin and 100 µg/ml streptomycin with additional 1 mM pyruvate. Both cell lines were cultured at 37°C with 5% CO_2 in a humidified incubator.

3.2.2 Passaging

Jurkat cells were maintained at a cell density between 0.2-1.0x10^6 cells/ml. For passaging, cell suspension was collected into a sterile tube and centrifuged (1000 rpm, 5 min, 20°C) and then washed with pre-warmed PBS before addition of new culture medium. HeLa cells were passaged until cells nearly reached confluency. Cells were washed with pre-warmed PBS and subsequently incubated with trypsin/ EDTA for 1-3 min at 37°C and then the tryptic digestion was stopped by adding new culture medium. After centrifugation (1000 rpm, 5 min, 20°C), the trypsin/EDTA solution was removed and replaced with new culture medium. For both of cell lines, the cell density was measured using the Vi-Cell™ XR cell viability analyzer and then the cells were plated into 75 cm^2 culture flasks or seeded in needed plates for further experiments.

Table 6 Solutions and reagents for cell culture

PBS (pH 7.4)	
NaCl	132.2 mM
Na_2HPO_4	10.4 mM
KH_2PO_4	3.2 mM
H_2O	

Trypsin/EDTA (T/E)	
Trypsin	0.05%
EDTA	0.02%
PBS	

3.2.3 Freezing and thawing

When the cell viability is relatively high, cells were collected with or without detachment as described in **3.2.2** and cells were re-suspended in ice-cold freezing medium at a cell density of 3.0x10^6 cells/ml. Then aliquot of 1 ml into cryovials were conducted and immediately frozen at -20°C for 30 min, stored at -80°C at least 24 h and finally transferred to liquid nitrogen (- 196°C) for long-term storage.

For thawing cells, the cryovials were thawed in a 37°C water bath and then were immediately transferred into 75 cm^2 flasks containing 10 ml pre-warmed culture medium and substituted with new culture medium on the next day.

3.2.4 Treatment of cells with compounds

Cells were seeded the night before treatment. DMSO solution was diluted in the corresponding culture medium and did not exceed 0.1% (v/v) in all experiments. Cells were incubated with compounds at indicated concentrations and time points.

3.3 Genomic Editing

3.3.1 Knockdown and overexpression

For gene silencing, cells were transfected with ON-TARGETplus Human EYA3 or BST-2 siRNA according to the manufacturer's instructions and ON-TARGETplus non-targeting control siRNA (NT siRNA) served as control. Briefly, HeLa cells were seeded in 6-well plates at a density of 0.42 million cells/well one day before transfection. 9 µl Lipofectamine RNAiMAX transfection reagent and 0.1 µM siRNA were diluted in 150 µl opti-MEM medium (Thermo Fisher Scientific, Cat# 31985070) respectively and mixed gently and then incubated for 5 min. siRNA solution was added into transfection reagent solution followed by a gentle mix and incubated for 15 min at room temperature (RT) before adding dropwise to HeLa cells. Following transfection, expression of EYA3 or BST-2 was determined with Western Blot using the EYA3 or BST-2 antibody.

For gene overexpression, cells were transfected with BST-2 plasmid or the empty vector plasmid as control. In brief, HeLa cells were seeded in 6-well plates at a density of 0.42 million cells/well one day before transfection. Lipofectamine 3000 reagent was diluted in opti-MEM Medium and the corresponding DNA was dispersed in opti-MEM Medium with addition P3000 reagent and then incubated for 5 min. Next, diluted DNA was added in the diluted Lipofectamine 3000 reagent and mixed well. After 15 min, the mixture was added to cells and cells were incubated at least 24 h. Following transfection, the overexpression efficiency was detected using Western blot with BST-2 antibody.

3.3.2 Establishment of HeLa BST-2 knockout (KO) cell lines

3.3.2.1 gRNAs design and Cloning and transformation of *E.coli*

gRNAs targeting human BST-2 was cloned into the vector PX459 V2.0 which was a gift from Feng Zhang[102] (Addgene plasmid # 62988; http://n2t.net/addgene:62988; RRID: Addgene_62988). Two gRNAs were used to increase KO efficiency, sequences of gRNA1: 5'-CGCTTATCCCCGTCTTCCAT-3', gRNA2: 5'-CCCCCAGAATCACGATGATC-3'. Single-strand gRNAs were dissolved in 100 µM annealing buffer (10 mM Tris pH 7.5, 50 mM NaCl and 1 mM EDTA) and then mixed with equal volumes of forward and reverse primers in a PCR tube. The mixture was then heated to 95°C for 2 min in a thermocycler and then was cooled gradiently to 25°C over 45 min. Meanwhile, the vector PX459 V2.0 was digested by restriction enzyme Bbsl (Table 7) at 37°C for 2 h and then annealed gRNAs were then ligated into the vector using T4 ligase (Table 7) at 4°C overnight respectively.

The ligation solution was transformed into DH5α. In brief, 50 µl DH5α competent cells were thawed on ice and 10 µl of the plasmid-DNAs solution was added and mixed well. The mixture was placed on ice for 30 min and heated at 42°C for 90 s, and then put on ice for another 2 min. Next, 300 µl LB medium was added into the tube and incubated at 37°C for 1 h. Finally, all bacterial suspension was plated on an agar plate containing 100 µg/mL ampicillin and incubated at 37°C for 1 h and then inverted for 12-16 h. Transformed DH5α colonies were picked and sequenced using human U6-forward primer 5'-GAGGGCCTATTTCCCATGATT-3'.

Table 7 Digestion and ligation

Digestion of vector	
Reagent	Amount (µL)
PX459 V2.0 vector	2
10 x FD buffer	2
Bbsl enzyme	0.2
Distilled H_2O	15.8

Ligation	
Reagent	Amount (µL)
Digested vector	5
insert	10
10x Ligase Buffer	2
T4 DNA Ligase enzyme	1
Distilled H_2O	2

3.3.2.2 Clonal isolation of cell lines and functional testing

HeLa cells were seeded into a 6-well plate and cell confluency was around 70% before transfection. Next day, cells were transfected with the plasmids using Lipofectamine 3000 for 2 days as described in **3.3.1** before puromycin selection (2 µg/ml) for another 2 days. Afterwards, the single cells isolation was performed with the serial dilution method. Briefly, the transfected cells were seeded 1 cell/ well into 96-well plates for 7-10 days in culture, and single-cell colonies were then expanded until cells were enough for freezing. To verify whether the candidates were true knockout clones, Western blot was used to detect the BST-2 protein level in wild type (WT) control cell and BST-2 knockout (KO) candidates, and then Flow cytometry was performed to detect the BST-2 surface level. Meanwhile, Full proteomics was applied to further confirm by Josef Braun (Group of Prof. Sieber, Department of Chemistry, Technical University of Munich, Germany) to check whether the BST-2 protein is completely depleted.

3.4 Cell proliferation assay

3.4.1 CellTiter Blue (CTB) assay

For investigating the effect of Lag A on the cell proliferation of Jurkat cells, CTB assay was performed. 5000 Jurkat cells/well were seeded into 96-well plates and on the

next day were stimulated with specific concentrations of Lag A or DMSO for 72 h and the final amount of medium in each well was 100 µl. Afterwards, 10 µl CTB reagent was added to each well for 2 h at 37 °C before fluorescence was determined using Ex:550 nm Em:595 nm by a SpectraFluor Plus™ microplate reader (Tecan, Crailsheim, Germany). Before normalization to DMSO control, day 0 values were subtracted in both experiments.

3.4.2 Crystal violet staining assay

To evaluate the proliferative capacity, crystal violet staining assay was performed to detect the effect of compounds on cell proliferation in HeLa cells, since HeLa cells are adherent. For the crystal violet staining assay, HeLa cells were seeded in 96-well plates at a density of 3000 cells/well the night before treatment and incubated with indicated concentrations of test compounds or DMSO. After 72 h, the medium was discarded and cells were washed with PBS and then stained with crystal violet solution (0.5% crystal violet, 20% methanol) for 10 min. Then cells were gently washed with water and dried followed by dissolving in sodium citrate solution (0.1 M sodium citrate, 50% ethanol). Absorbance was measured at 550 nm by a Sunrise™ microplate reader (Tecan, Crailsheim, Germany). For analysis, values of the day 0 were subtracted, and results were normalized to the DMSO control which was set to 100% proliferation.

3.5 Flow cytometry

3.5.1 Apoptosis assay

Cell apoptosis was detected using Nicoletti assay and Flow cytometry as described by Nicoletti et al.[103]. In brief, the day before treatment, 0.1 million cells/well were seeded into 12-well plates and treated with specific concentrations of compounds or DMSO on the next day. After 24 h or 48 h incubation time, cells were harvested and washed with pre-cooled PBS. Then cells were stained with Nicoletti buffer (0.1% sodium

citrate, 0.1% Triton X-100) containing 50 µg/ml PI and incubated at 4°C for 30 min in the dark. The percentage of apoptotic cells was measured at Ex:488 nm Em:585 nm by FACSCanto II (BD, New Jersey, USA) and 10,000 events were analyzed in each sample.

3.5.2 Mitochondrial membrane potential measurement

Mitochondrial membrane potential (ΔΨm) was determined by JC-1 staining according to the manufacturer's instructions. In detail, 0.1 million cells/well were seeded into 12-well plates overnight and stimulated with indicated concentrations of Lag A or DMSO. CCCP served as the positive control. After 24 h, cells were harvested and washed with PBS and then incubated with 1 µg/ml JC-1 working solution at 37°C for 20 min in the dark (the suspension was shaked periodically). Subsequently, cells were washed with PBS and resuspended in 200-300 µl PBS. The relative percentage of populations exposing red or green fluorescence was measured by FACSCanto II and 10,000 events were analyzed in per sample. Meanwhile, the compensation set up was determined by using compensation samples of the BD CompBeads Anti-mouse Ig, κ particles set and Alexa Fluor 488 and PE-conjugated antibodies according to the manufacturer**.**

3.5.3 Detection of Reactive oxygen species release

Reactive oxygen species (ROS) release was detected using carboxy-H_2DCFDA (6-carboxy-2',7'-dichlorodihydrofluorescein diacetate) probe staining and Flow cytometry. In brief, 0.2 million cells/well were seeded into 12-well plates the day before treatment and stimulated with indicated concentrations of compounds or DMSO on the following day for 24 h. CCCP served as the positive control. Cells were collected by centrifugation and washed with PBS and then stained with Carboxy-H_2DCFDA (10 µM) at 37°C in the dark. After 30 min, cells were washed with PBS to remove excess dye and resuspended in PBS followed by immediately analysis at Ex:488 nm Em:530 nm by FACSCanto II. 10,000 events were analyzed in

each sample.

3.5.4 Detection of BST-2 surface level

To analyze the effect of NCA on BST-2 surface level, Flow cytometry was used. 0.1 million cells per well were seeded into 12 well plates. After indicated treatment of compounds, cells were trypsinized and collected into 15 ml falcon tubes, and then cells were washed by centrifugation (350 g, 5 min at 4°C) in PBS. Next, cells were resuspended in 150 µl of diluted primary antibody, which was diluted in Antibody dilution buffer (1% FCS in PBS, 1:200 dilution) and incubated on ice in a shaker shaking gently for 1 h in the dark. Subsequently, cells were washed twice by centrifugation (350 g, 5 min at 4°C) in pre-chilled PBS to remove the excess antibody and then resuspended in 100 µl of diluted Alexa Fluor 488-conjugated secondary antibody (prepared in Antibody dilution buffer). After 30 min incubation on ice in the dark, the cells were washed twice by centrifugation (350 g, 5 min at 4°C) in pre-chilled PBS to remove excess dye and finally resuspended in 200-500 µl of pre-cooled PBS and analyzed on Flow cytometer. In parallel, the anti-mouse IgG served as isotype control.

3.6 Detection of ATP production

CellTiter Glo kit was used to investigate the effect of Lag A on ATP production. 5,000 cells/well in 100 µl were plated into 96-well plates and allowed to adhere overnight. Cells were treated with subtoxic concentrations of Lag A or DMSO for 24 h and plates were equilibrated at RT for 30 min before 100 µl of CellTiter Glo reagent was added to each well. After 2 min of shaking and 10 min of incubating at RT, the values of luminescence intensity were recorded by the Tecan Sunrise microplate reader. Before normalization to DMSO control, the values of control wells containing medium without cells were subtracted.

3.7 Transmission Electron microscopy

0.3 million cells/well were seeded into 6-well plates the night before stimulation and

then treated with Lag A or DMSO for 24 h. Cells were detached and washed with PBS once before 0.45 million cells/well in each group were plated into BEEM® capsules. Subsequently, the supernatant was removed after centrifugation, and cells were incubated with 600 µl 2.5% glutaraldehyde (EMS Science Services, Hatfield, PA, USA) in 0.1 M sodium cacodylate buffer (pH 7.4). Embedding and further preparation of the samples was performed by Carola Eberhagen and electron microscopy was performed by Dr. Sabine Schmitt in the laboratory of Prof. Dr. Hans Zischka (Institute of Molecular Toxicology and Pharmacology, Helmholtz Centre, Munich).

3.8 Seahorse mitostress test

1.2 x 10^4 HeLa cells/well were seeded into XFe 96 microplates (Agilent Technologies, Santa Clara, USA) and allowed to adhere overnight prior to specific compounds treatment for 24 h. Subsequently, the Seahorse mitostress test was performed according to the manufacturer's protocol (#103020-400, #103015-100) in the Seahorse XFe96 Analyzer (Agilent Technologies, Santa Clara, USA). Briefly, cells were pre-treated with Lag A for 24 h and then Oligomycin, FCCP, and a combination of Rotenone and Antimycin A (Rot/AA) were added automatically into the Seahorse cartridge at the indicated time points. Meanwhile, cell number was measured by the CyQuant® GR dye DNA content measurement and the data were normalized to the corresponding cell number in each well.

3.9 Western Blot

3.9.1 Subcellular Fractionation

HeLa cells were seeded in 10-cm petri dishes overnight and on the next day were treated with different concentrations of Lag A for 24 h. According to the subcellular fractionation protocol from Abcam, cells were harvested and lysed using 500 µl of lysis buffer and then scraped immediately followed bypassed through a 25 Ga needle 10 times. After incubation on ice for 20 min and centrifugation, the nuclear pellet and supernatant were used to further isolate the nuclear fraction and mitochondrial

fraction. For nuclear fraction, the pellet was resuspended in 500 µl of lysis buffer and passed through a 25 Ga needle 10 times again. The supernatant was removed after centrifugation and the pellet was resuspended in the nuclear buffer (lysis buffer with addition 10% glycerol and 0.1% SDS) and then sonicated briefly. For mitochondrial fraction, the supernatant was centrifuged again and then the pellet was resuspended in 500 µl of lysis buffer followed by the same steps as with the nuclear pellet to get the mitochondrial fraction.

3.9.2 Cell lysis preparation

Cells were seeded into 6-well plates at a density of 0.42 million cells/well and treated with indicated concentrations and time points of compounds or siRNA. Cells were harvested and washed with cold PBS prior to addition of lysis buffer (Table 8) and frozen at -80°C overnight. Next, before cells were scraped off with a cell scraper and transferred into 1.5 ml tubes, cells were incubated for at least 30 min on ice. After centrifugation (10.000 g, 10 min, 4°C), the supernatants were collected for the further experiment and then the samples were stored at -20°C.

Table 8 Buffers for cell lysis

Lysis buffer (pH 7.5)			
Na_2EDTA	2 mM	Na_2-β-Glycerophosphate	20 mM
NaCl	137 mM	NaF	10 mM
Glycerol	10% (v/v)	Add before use:	
$Na_4P_2O_7$	2 mM	PMSF	1 mM
Tris-Base	20 mM	Complete (25x)	4% (v/v)
Triton X-100	1% (v/v)	Na_3VO_4	2 mM

3.9.3 Protein concentration detection and sample preparation

To determine the concentration of each sample and make sure equal protein load, protein concentration was measured by Bradford assay. First, each cell lysate was diluted in water (1:5 dilution) and mixed well and then 10 µl of the diluted solution or

bovine serum albumin (BSA) standards (c=0-500 µg/ml) were transferred to a 96-well plate in triplicates. 190 µl diluted Bradford reagent (1:5) was added to each well and incubated for 5 min at RT in the dark. The absorbance was measured at a Tecan Sunrise microplate reader and protein concentrations of the samples were determined by linear regression. Finally, each cell lysate was mixed with 5xSDS sample buffer (Table 9) and adjusted by adding 1xSDS sample buffer (1:5 dilution in distilled H_2O). Before being resolved by SDS-polyacrylamide gel electrophoresis (SDS-PAGE), the samples were boiled at 95°C for 10 min.

Table 9 Sample buffers for Western blot

5x Sample Buffer	
Tris-Base pH 6.8 3.125M	10% (v/v)
Glycerol	50% (v/v)
20% SDS	25% (v/v)
16% DTT	25% (v/v)
2.5% Pyronin Y	1% (v/v)
Distilled H_2O	

3.9.4 SDS-polyacrylamide gel electrophoresis (SDS-PAGE) and protein detection

Next, equal amounts of protein were separated by SDS-polyacrylamide gel electrophoresis (SDS-PAGE) on discontinuous polyacrylamide gels (Table 10) in electrophoresis buffer (Table 10) (80 V 30 min and then 120 V 40 min) and transferred to 0.22 µm PVDF membrane in 1xTANK buffer (Table 11) (110 V, 90 min). Membranes were blocked with 5% (w/v) BSA in TBS-T buffer (24.8 mM Tris base, 190 mM NaCl, and 0.1% Tween-20) for 2 h at RT and subsequently incubated with appropriate primary antibodies overnight at 4°C. The membranes were washed with TBS-T three times before incubating with HRP-conjugated secondary antibodies for 2 h at RT. After washing again with TBS-T, the chemiluminescence was visualized by incubating membranes with ECL solution (100 mM pH 8.5 Tris, 2.5 mM Luminol, 1

mM Coumaric acid, and 17 mM H_2O_2) before using a ChemiDoc™ touch imaging system.

Table 10 Buffers and gel mixtures for gel electrophoresis

Stacking Gel	
Rotiphorese Gel 30	17% (v/v)
Tris-HCl pH 6.8	125 mM
SDS	0.1% (w/v)
TEMED	0.2% (v/v)
APS	0.1% (w/v)
Distilled H_2O	

Separation Gel 12%	
Rotiphorese Gel 30	40% (v/v)
Tris-HCl pH 8.8	375 mM
SDS	0.1% (w/v)
TEMED	0.1% (v/v)
APS	0.05% (w/v)
TCE	0.5% (v/v)
Distilled H_2O	

Electrophoresis buffer			
Tris	4.9 mM	SDS	0.1% (w/v)
Glycine	38 mM	Distilled H_2O	

Table 11 Buffers for tank blotting

5x tank buffer	
Tris base	240 mM
Glycine	195 mM
Distilled H_2O	

1x tank buffer	
5x tank buffer	20% (v/v)
Methanol	20% (v/v)
Distilled H_2O	

3.10 Immunofluorescence staining assay

3.10.1 Mitochondria staining

HeLa cells were seeded in ibidi 8-well µ-slides and allowed to adhere overnight. After the corresponding treatment of compounds or DMSO, cells were washed with PBS and incubated with the pre-warmed MitoTracker™ deep red staining solution (1:10,000 dilution) for 30 min at 37 °C incubator and then stained with Hoechst 33342

(5 µg/ml) for another 30 min, followed by washing with pre-warmed PBS. After fixation in 4% (v/v) paraformaldehyde (PFA) for 10 min and washed with PBS, cells were covered with FluorSave reagent mounting medium and glass coverslips. Images were captured by confocal microscopy with a Leica SP8 LSM system and the fluorescence intensity was analyzed with ImageJ software.

3.10.2 DNA damage repair foci staining

To investigate the change of DNA damage repair process, γH2AX (a marker for detecting the DNA damage and repair process) staining was used. Cells were seeded in ibidi 8-well µ-slides and incubated overnight. After indicated treatment, cells were washed with PBS and fixed with 4% (v/v) PFA in PBS for 10 min and then permeabilized with 0.5% Triton X-100 for 15 min at RT. The cells were washed with PBS and blocked in 1% (w/v) BSA in PBS for 1 h at RT followed by incubating with γH2AX antibody (1:200 dilution) overnight at 4°C. On the next day, cells were washed three times with PBS containing 0.2% Triton X-100 and then incubated with Alexa fluor 488 coupled secondary antibody (1:400 dilution) and Hoechst 33342 (5 µg/ml) for 1 h at RT. Cells were submerged with one drop of FluorSave reagent mounting medium and covered with a glass coverslip after being washed again with PBS three times. Images were captured by confocal microscopy.

3.10.3 Fluorescence recovery after photobleaching (FRAP)

0.42 million cells were seeded into 6-well plates and incubated overnight. Cells were transfected with GFP tagged EGFR plasmid using Lipofectamine™ 3000. After 24 h, cells were re-seeded in ibidi 8-well µ-slides and allowed to adhere overnight before the indicated treatment. After stimulation, cells were immediately imaged live and the FRAP experiment was conducted on a Leica SP8 confocal microscope with the HC PL APO CS2 63x/1.4 NA oil objective and the heating and gas incubation system from Okolab ensuring constant 37°C under 5% CO_2 and 80% humidity. In detail, the initial fluorescence was measured in the region of interest (Fi). Next, the fluorescent

molecules were photobleached within a selected area. As a result, a dark area was observed (F0). Finally, fluorescent molecules from the surroundings diffused through the sample and exchanged the photobleached molecules with intact ones (F∞). With the LAS X Core Software, the FRAP settings were adjusted to one pre-bleach iteration, 60 bleach iterations, five post-bleach iterations with 30 sec intervals and 15 with 60 sec intervals. Images were taken with a pinhole size adjusted to 1.0 airy units and a scanning speed of 400 Hz. This fluorescence recovery was measured over time. For the analysis, the mobile fraction R was calculated as: $\mathrm{R} = (\mathrm{F}\infty - \mathrm{F0})/(\mathrm{Fi} - \mathrm{F0})$

3.10.4 Lipid rafts staining

Cells were seeded in ibidi 8-well µ-slides overnight before indicated treatment. Cells were washed with chilled complete growth medium and incubated with the fluorescent CT-B conjugate working solution (1 µg/mL in chilled complete growth medium). After 10 min at 4°C, cells were washed gently with chilled PBS three times. Afterwards, cells were incubated with the chilled anti-CT-B antibody working solution (1:200 dilution) for 15 min at 4°C. After this incubation, cells were washed gently with chilled PBS before fixation in chilled 4% PFA for 15 min at 4°C. The following steps were as described in **3.10.2**.

3.11 Quantitative real-time PCR analysis

Cells were treated with compounds or DMSO for indicated time points and mRNA from each well was isolated using the RNeasy® Mini Kit according to the manufacturer. The mRNA concentration was determined by a Nanodrop® Spectrophotometer followed by reverse transcription of mRNA to cDNA with the High-Capacity cDNA Reverse Transcription Kit (Applied Biosystems, Waltham, USA) as described by the manufacturer. Subsequently, the quantitative real-time polymerase chain reaction (qPCR) was performed and a QuantStudio™ 3 Real-Time PCR System was used. In brief, primers were designed using the Harvard primer bank (https://pga.mgh.harvard.edu/primerbank/) and the forward and reverse primers for GAPDH gene (FW：GGAGCGAGATCCCTCCAAAAT, RE：

GGCTGTTGTCATACTTCTCATGG), for the BST-2 gene (FW: CACACTGTGATGGCCCTAATG, RE: GTCCGCGATTCTCACGCTT). After the synthesis of the primers from Metabion (Planegg, Germany), the qPCR reaction solution was added in each well of the MicroAmp® Fast Optical 96-Well Reaction Plate and foil was sealed and then the plate was centrifuged (1000 rpm, 1 min). Afterwards, the qPCR process was performed. For the data analysis, GAPDH served as control gene and the $\Delta\Delta C_T$ method was used to quantify changes in mRNA levels.

3.12 QUANTIFICATION AND STATISTICAL ANALYSIS

All repeated experiments are independent and biological replicates unless indicated otherwise. Flow cytometry data were processed with FlowJo 7.6. Confocal images and Western blot densitometry were analyzed using ImageJ. Statistical analyses were performed with GraphPad Prism 8/9. Ordinary one-way ANOVA with a post-hoc Tukey's test or Dunnett's test was performed and significance is showed as $^{ns}p > 0.12$, *p<0.033, **p<0.002, ***p<0.001. All shown graphs are presented as means ±standard error of mean (SEM). Bliss synergy score was calculated according to the Bliss independence model and the equitation is $S_{BLISS} = E_{A,B} - (E_A + E_B - E_A E_B)$, where S_{BLISS}<0:antagonism, $S_{BLISS} = 0$: additive, S_{BLISS}>0: synergistic.

RESULTS PART I
---LAGUNAMIDE A

4. Results-Part I

4.1 Lag A inhibits cancer cell proliferation and promotes cancer cell apoptosis.

As previously shown, Lag A has potent growth inhibitory effect towards tumor cells[18]. To investigate the effect of Lag A on cell proliferation in HeLa and Jurkat cells, crystal violet staining assay and CTB assay were performed respectively. The proliferation of both cell lines was significantly inhibited in a nanomolar range of Lag A treatment and the half maximal inhibitory concentration (IC_{50}) values of Lag A against HeLa and Jurkat cells were 19.41 nM and 7.898 nM respectively (Figure 5A and 5B). As shown in Figure 5C and 5D, the percentage of apoptotic cells was increased by Lag A stimulation in both cell lines compared to DMSO control and the concentration for 50% of maximal effect (EC_{50}) values of Lag A against HeLa and Jurkat cells were 40.50 and 5.561 nM respectively. Besides, to better gain more insight into the potential of this interesting compound class, structure-activity relationship study (SAR) was performed to determine the anti-proliferative and pro-apoptotic effects of Lag A and its analogues (Supplementary Figure 1). Taken together, these data reveal that Lag A exerts its anti-tumor effect through affecting cell proliferation and cell apoptosis.

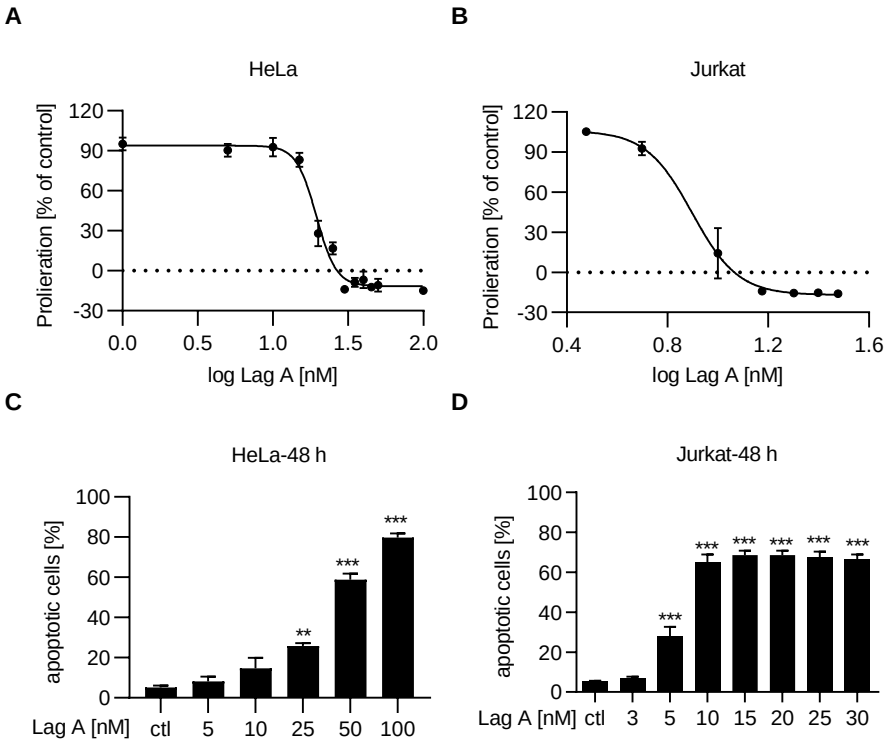

Figure 5. Lag A inhibits cell proliferation and promotes cell apoptosis in HeLa and Jurkat cells. (A) Effect of Lag A on cell proliferation in HeLa cells was measured by crystal violet staining assay after indicated treatment for 72 h. The

percentage of cells was normalized to DMSO control. Data are plotted as the means ± SEM, n=3. (B) Effect of Lag A on cell proliferation in Jurkat cells was measured by CTB assay (since the crystal violet assay is not applicable for suspension cells) after indicated treatment for 72 h. Data are presented as means ± SEM, n=3. (C) Effect of Lag A on cell apoptosis in HeLa cells was detected by Nicoletti assay after treatment with different concentrations for 48 h. Data are presented as means ± SEM, n=3, one-way ANOVA, Dunnett's test, **P<0.002, ***P<0.001. (D) As in (C), except the cell line was Jurkat cell.

4.2 Lag A causes severe mitochondrial dysfunction.

Since Aurilide, a natural compound, which is structurally closely related to Lag A (Figure 2), has been demonstrated to elicit its cellular effects via alteration of mitochondrial function, we also investigated mitochondrial effects of Lag A. By transmission electron microscopy (TEM) we clearly saw a change of mitochondrial morphology after Lag A treatment. The mitochondrial morphology in the control group showed a structurally intact outer membrane and clearly visible cristae structure while mitochondria became much smaller with an extremely condensed matrix after treatment with Lag A (Figure 6A). Moreover, to confirm this change, HeLa cells were stained with MitoTracker™ deep red and subsequently confocal microscopy was applied. As expected, Lag A caused similar mitochondrial morphological alteration with fragmentation of mitochondria and increased fission compared to the mitochondrial morphology of DMSO control (Figure 6B).

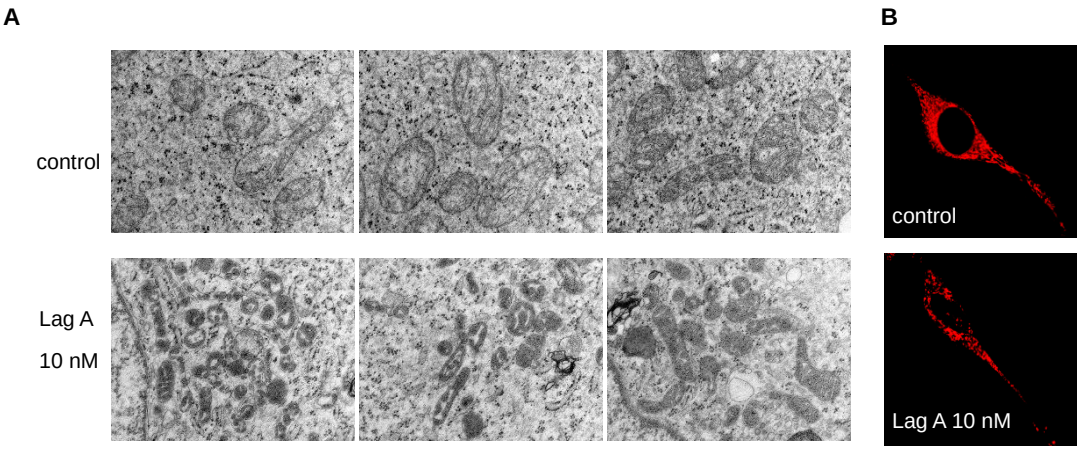

Figure 6. Lag A affects mitochondrial morphology. Mitochondrial morphology alterations were detected using Transmission electron microscopy (A) and MitoTracker™ deep red staining (B) in 24 h Lag A treated-cells. Representative images are from one of three independent experiments. Scale bar represents 500 nm and 10 µm for (A) and (B) respectively. (A) was conducted by Dr. Sabine Schmitt in the laboratory of Prof. Dr. Hans Zischka (Institute of Molecular Toxicology and Pharmacology, Helmholtz Centre, Munich) and (B) was performed by Christina Orgler (PhD Thesis).

Based on this change, we further investigated the effect of Lag A on biochemical mitochondrial function. As shown in Figure 7A, subtoxic concentrations of Lag A led to robust reduction in the ratio of ATP production compared to DMSO control. Besides, Lag A also induced a dramatic increase in the percentage of the JC-1 monomer population, which indicated a drop in mitochondrial membrane potential (MMP, ΔΨm) (Figure 7B) that is another key indicator of mitochondrial activity and influences the production of ATP as well as of reactive oxygen species (ROS). ROS were elevated in both HeLa and Jurkat cells upon Lag A treatment (Figure 7C and 7D).

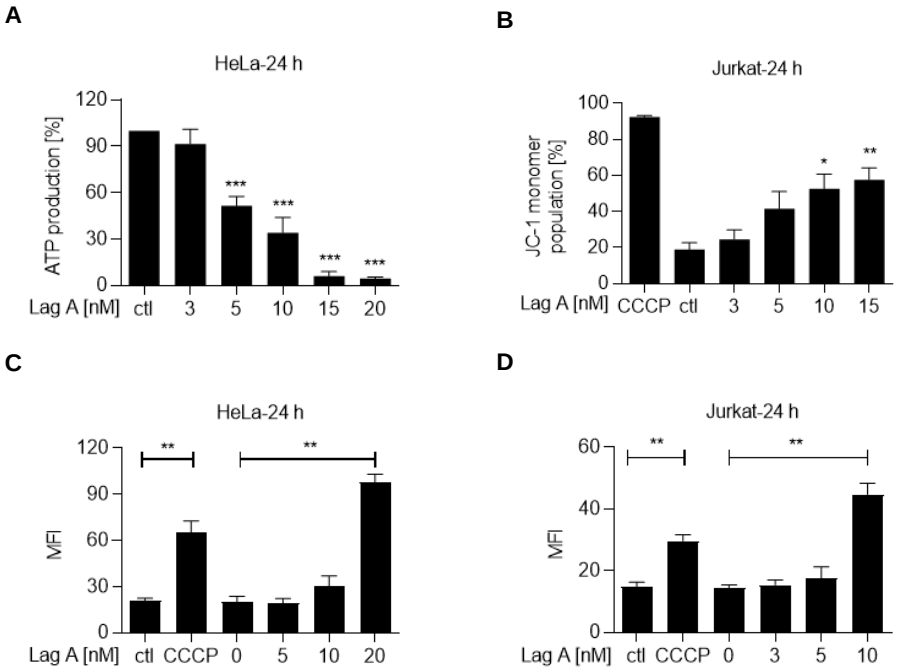

Figure 7. Lag A influences ATP production and MMP accompanied by the release of ROS. (A) ATP production measurement in HeLa cells using CellTiter Glo kit, following 24 h of indicated treatment with Lag A. Culture medium values were subtracted as blanks from each well and the percentages of ATP production were normalized to DMSO control. The values are means ± SEM, n=3 (one-way ANOVA, Dunnett's test, ***P<0.001). (B) Mitochondrial membrane potential of Jurkat cells treated with indicated concentrations of Lag A for 24 h was measured by JC-1 staining and FACS analysis. Data are plotted as the means ± SEM, n=3. (one-way ANOVA, Dunnett's test, *p<0.033, **P<0.002). (C) Production of intercellular reactive oxygen species (ROS) in HeLa cells treated with indicated compounds for 24 h was detected by carboxy-H_2DCFDA staining and FACS analysis. DMSO and CCCP served as control and positive control respectively. Data are plotted as the means ± SEM, n=3. (one-way ANOVA, Dunnett's test, **P<0.002). (D) Production of intercellular reactive oxygen species (ROS) in Jurkat cells treated with indicated compounds for 24 h was detected by carboxy-H_2DCFDA staining and FACS analysis.

Furthermore, to better understand effects of Lag A on mitochondrial respiration,

cellular oxygen consumption rate (OCR) was monitored using a Seahorse Extracellular Flux analyzer. Firstly, the basal respiration was decreased with 10 nM Lag A treatment before adding any inhibitors, and this effect suggested that Lag A led to a decrease in oxidative phosphorylation. Then oligomycin, an ATP synthase inhibitor, was added, which reduced mitochondrial oxygen consumption and a drop of ATP production with Lag A treatment was detected. Next, addition of FCCP uncoupled oxygen consumption from ATP production by disrupting the mitochondrial the proton gradient and resulting in maximal oxygen consumption. Under this condition, the maximal respiration was reduced upon Lag A treatment. These results were consistent with decreases in ATP-linked respiration. By the final injection of rotenone (Rot) and Antimycin A (AA), the electron transport chain was targeted, thereby reducing OCR to a minimum value (Figure 8).

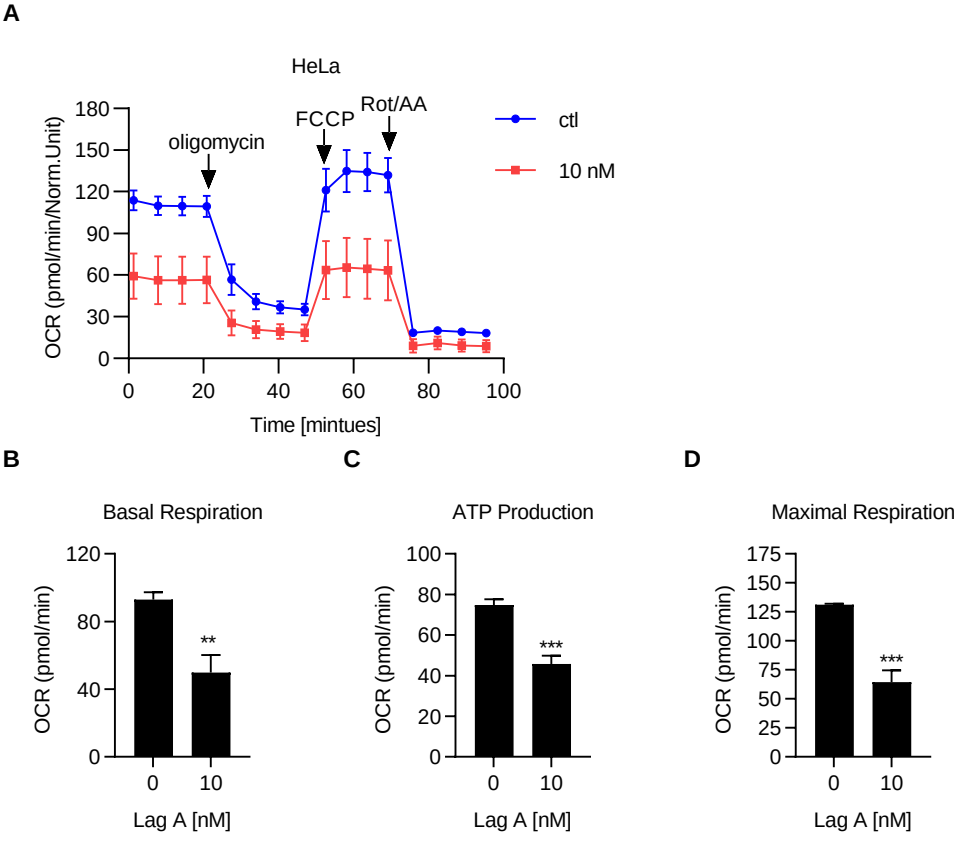

Figure 8. Lag A decreases oxygen consumption rate (OCR). (A) Oxygen consumption rates detection using a Seahorse Extracellular Flux analyzer after indicated treatment with Lag A. Line graph shows the real-time OCR profile plot. Results are the mean of three independent replicates and error bars represent SEM. (B, C and D) Detailed analysis from the real-time OCR profile plot. B: basal respiration; C: ATP production; D: maximal respiration. Bar represent the means ± SEM, n=3, one-way ANOVA, Dunnett's test, **P<0.002, ***P<0.001. Experiments were conducted by Christina Orgler (PhD Thesis).

In view of the alteration in mitochondrial morphology and function after Lag A treatment, key mitochondrial related proteins were evaluated. As shown in Figure 9A, notably, OPA-1 and Mfn-1, important proteins for maintaining mitochondrial fusion and fission[104], were obviously reduced by Lag A treatment, which was consistent with the mitochondrial morphological alteration. Besides, Lag A markedly down-regulated the expression levels of the anti-apoptotic Bcl-2 family proteins including Bcl-2, Bcl-xl and Mcl-1. In addition, to decipher whether Lag A promotes cell apoptosis through the mitochondrial pathway, cytochrome C release from mitochondria was detected using subcellular fractionation after Lag A treatment, and Lag A caused a significant reduction of cytochrome C from mitochondria accompanied with an increase of the protein in the cytosolic fraction (Figure 9B). Thus, these data indicate that Lag A impairs mitochondrial function.

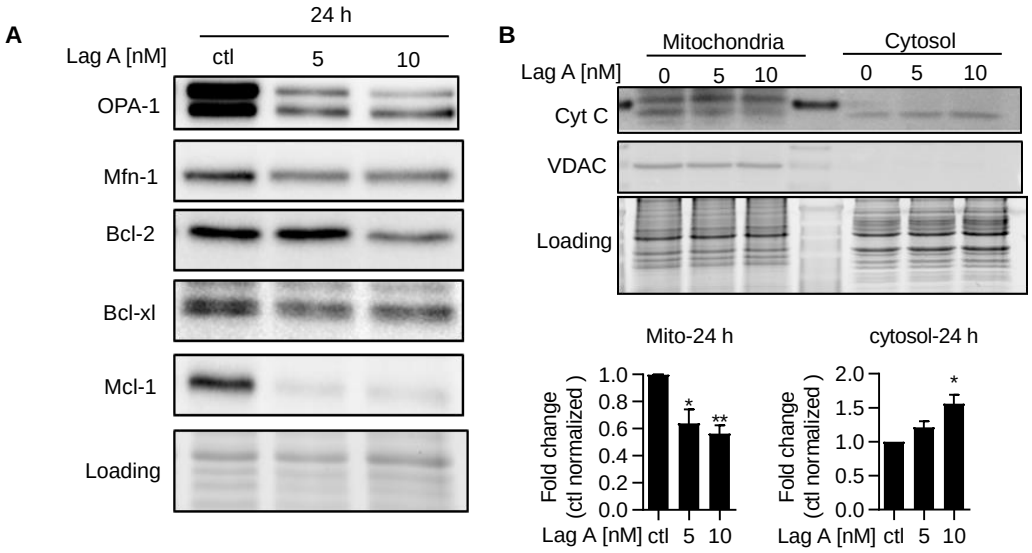

Figure 9. Lag A influences mitochondrial apoptotic pathway. (A) Western blot of mitochondrial related proteins, including OPA-1, Mfn-1, Bcl-2, Bcl-xl and Mcl-1 after 24 h of treatment with Lag A. Representative images are selected from one of three independent experiments. This experiment was conducted by Christina Orgler (PhD Thesis). (B) Cytochrome C release from mitochondria to cytosol was measured by sub-cellular fractionation of HeLa cells treated with Lag A for 24 h and Western blot. VDAC served as a marker of mitochondria. Bar graphs indicate the expression level of cytochrome C in mitochondria and cytosol analyzed by ImageJ. Data are plotted as the means ± SEM, n=3. (one-way ANOVA, Dunnett's test, *p<0.033, **P<0.002).

4.3 Thermal proteome profiling allows target identification of Lag A

To identify the protein targets of Lag A, we synthesized affinity-based probes bearing a photo crosslinking moiety for covalent attachment to the target proteins and an alkyne moiety for attachment of an enrichment handle (Supplementary Figure 2) via

copper catalyzed azide alkyne cycloaddition (CuAAC). As the natural product Lag A bears a phenyl moiety, the most straight forward way to introduce a photo cross linker was to convert the phenyl ring to an aryl-azide moiety. The alkyne moiety was introduced via an ether adjacent to the macrolacton ester. As in our previously reported synthesis of Lag A[105], we built up the stereocenters of the modified polyketide part via iterative Matteson homologations (Supplementary Figure 2A). The potency of the photo affinity probe concerning anti-proliferative action was reduced by approx.a factor of 200 as compared to Lag A (Supplementary Figure 2A), nevertheless it was still in the nanomolar range, which encouraged us to go ahead with proteomic studies in living cells. Surprisingly, the new probes were only taken up slowly, necessitating long incubation times (data not shown). After labelling, CuAAC to biotin-azide, enrichment using avidin beads, tryptic digest and LC-MS/MS, there were no reproducibly enriched protein targets detected. To overcome the slow uptake, we also performed these experiments in cell lysate (Supplementary Figure 2B). This also did not produce any enriched proteins. To investigate any potential reasons as to why no proteins were enriched, such as the probe not being stable during enrichment, the protocol was repeated using a trifunctional linker bearing an azide-, biotin- and a rhodamine-moiety. This allows both visualization via fluorescence after SDS-PAGE, but also enrichment of labelled proteins. The resulting SDS-gel was imaged for fluorescence and also stained with Coomassie to visualize all proteins. This experiment demonstrates that the observed photo-crosslinking seems to be unspecific (Supplementary Figure 2C). One would expect the relative abundance of proteins to change after enrichment with avidin beads. This was not the case in this experiment, as can be seen in the Coomassie stained gel (Supplementary Figure 2D). The affinity-based probe is therefore not suitable for target identification of Lag A.

To overcome the limitations of affinity-based proteome profiling we performed thermal proteome profiling (TPP) using the natural product Lag A. Jurkat cells were treated in situ with 500 nM Lag A or vehicle control and were exposed to a temperature gradient. After lysis and isolation of the soluble fraction by ultracentrifugation the proteomes were digested and subsequently labelled with tandem mass tags (TMT). After

labelling the different temperature points with different TMT-channels, the 10 different temperature points were combined and then fractionated by hydrophilic interaction chromatography (HILIC). The fractions were analyzed by LC-MS/MS/MS (Figure 10A). The Tm shifts were calculated for both replicates and plotted after filtering (Figure 10B). Four proteins were stabilized by more than 2.5°C in both Lag A treated samples and passed all additional significance thresholds, while three proteins were destabilized by more than 2.5°C and passed all additional significance thresholds. Among the three stabilized proteins were EYA3 (eyes absent homolog 3), SMC1A (Structural maintenance of chromosomes protein 1A) and NDC80 (Kinetochore Protein NDC80 Homolog). EYA3 and SMC1A both play a role in DNA damage repair, while NDC80 organizes and stabilizes microtubule-kinetochore interactions. Amongst them, EYA3 attracted our attention and the thermal response curve of target protein EYA3 was shown in Figure 10C.

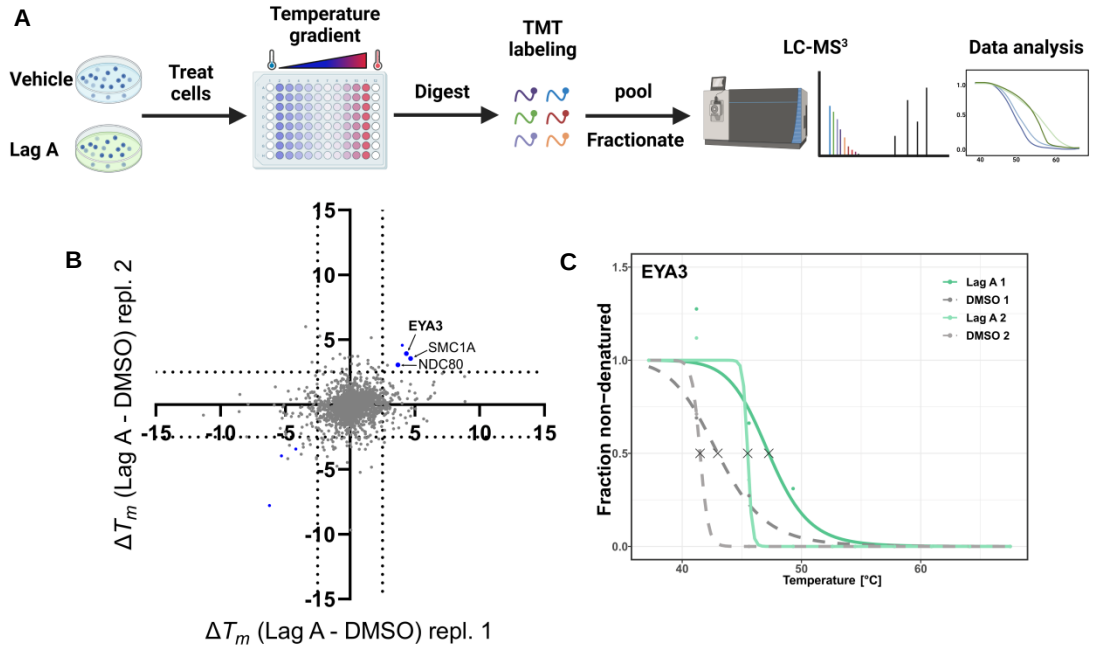

Figure 10. Target Identification of Lag A using thermal protein profiling. (A) Schematic workflow of the thermal proteome profiling experiment. Living Jurkat cells were treated with 500 nM of Lag A or DMSO for 1 h. Subsequently, aliquots were incubated at 10 different temperatures ranging from 37°C to 67°C. After isolating the soluble fraction via centrifugation, the proteins were digested and TMT labelled before being fractionated and analysed by mass spectrometry. (B) Scatter plot of the calculated thermal shifts (ΔT_m) between vehicle and Lag A treated cells. Proteins that have passed all significance criteria are displayed in blue. Samples were measured using MS3 based reporter ion quantification and raw data was analysed using MaxQuant. Thermal response curve fitting as well as melting points

were calculated using the TPP R package. (C) Thermal response curve of target protein EYA3. Lag A treated samples are displayed in green while Vehicle treated samples are displayed in grey. The melting points (Tm) are marked by a X. Experiments were performed by Dietrich Mostert (Group of Prof. Sieber, Department of Chemistry, Technical University of Munich, Germany).

4.4 Lag A inhibits formation of DNA damage repair foci after treatment with DXR via interaction with EYA3.

Among the potential targets of Lag A elicited by TPP, EYA3 was first investigated and for validation of the proposed targets, genetic depletion of EYA3 was applied, but unfortunately EYA3 knockdown (KD) showed only limited impact on antagonizing the anti-proliferative and pro-apoptotic effect of Lag A (Supplementary Figure 3). However, EYA3 is essential for the DNA damage repair process[57]. Here, doxorubicin (DXR), a widely used chemotherapeutic drug and DNA damaging agent[106], was chosen to establish a DNA damage. To monitor the DNA damage and repair process, the change of γH2AX (phosphorylation of histone H2AX at Ser139), an early cellular response to the induction of DNA double-strand breaks, was selected as a marker[107]. In order to detect the effect of Lag A on the DNA damage repair process, immunofluorescence staining was used. As expected, DXR treatment induced a strong increase of γH2AX intensity, whereas surprisingly, nearly no fluorescence of γH2AX was detected after Lag A pre-treatment and a significant decrease on the γH2AX intensity in combination treatment group compared to the DXR treatment group (Figure 11A and 11B). To confirm the phenotype, the relative protein level of γH2AX was investigated using Western blot. In good accordance with the staining results, the expression level of γH2AX was increased significantly upon DXR treatment, and with Lag A combination treatment, the γH2AX expression levels were reduced (Figure 11C and 11D). It is a widely-accepted concept that after DNA damage, cells need to decide, whether DNA repair is possible, or whether they are beyond repair and should undergo apoptosis[108]. Therefore, we next examined, whether Lag A influenced this decision and acted synergistically with DXR on cell apoptosis. As expected, HeLa cells showed a significant increase of the percentage of apoptotic cells in response to treatment with subtoxic dose of Lag A in combination

with DXR compared to Lag A or DXR treatment alone (Figure 11E). The Bliss scores calculated according to Bliss independence model were over 10 (Supplementary Table 1), and this indicated the synergistic effect of Lag A in combination with DXR. Thus, HeLa cells pre-treated with Lag A were more sensitive to DXR-induced DNA damage.

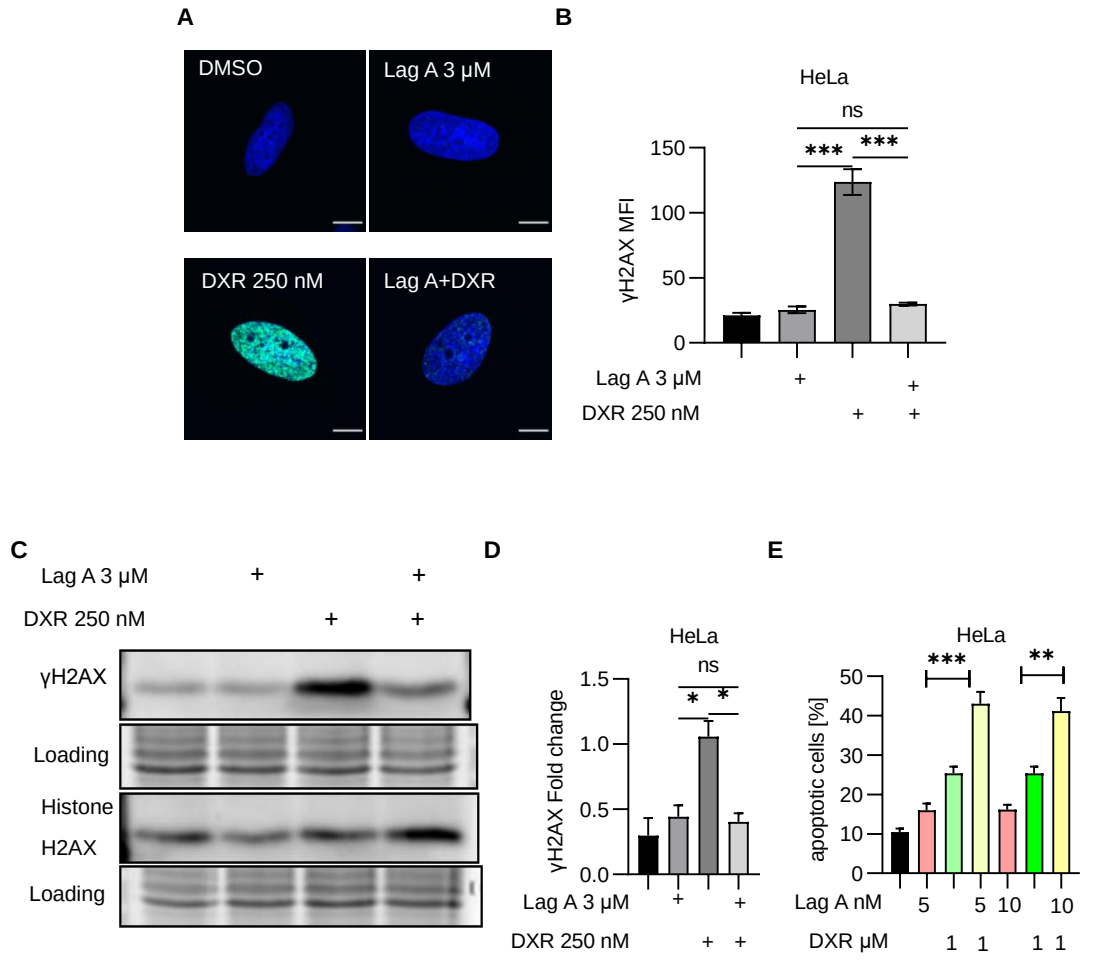

Figure 11. Lag A inhibits formation of DNA damage repair foci after treatment with doxorubicin via interaction with EYA3. (A) Immunofluorescence images of γH2AX (green) and Hoechst 33342 as nuclear counter stain (blue) in treated HeLa cells. Cells were pre-treated with 3 µM Lag A for 1 h before 250 nM DXR was added for another 2 h and then medium was changed into fresh medium for 1 h. Scale bar represents 10 µm. (B) Bar graph shows the mean fluorescence intensity of γH2AX from three independent experiments using ImageJ and at least 70 cells were collected in each group for quantitative analysis. The values are means ± SEM, n=3 (one-way ANOVA, Tukey's test, $^{ns}p>0.12$, ***P<0.001). (C) Western blot of γH2AX and Histone H2AX after treatments as described in (A). The shown images are from one of three independent replicates. (D) Immunoblot quantification of γH2AX expression level normalized to Histone H2AX using ImageJ. Data are presented as means ± SEM, n=3, one-way ANOVA, Tukey's test, $^{ns}p>0.12$, **P<0.002. (E) Effect of Lag A on DXR-induced cell apoptosis was determined by Nicoletti assay. HeLa cells were treated with indicated concentrations of Lag A for 24 h followed by stimulation with DXR for another 24 h. Error bars represent SEM, n=3, one-way ANOVA, Tukey's test, **P<0.002, ***P<0.001.

To validate whether EYA3 is the responsible target of Lag A for inhibiting DNA damage repair, genetic knockdown was used. As shown in Figure 12A, the inhibitory effect of Lag A on γH2AX intensity after treatment with DXR, was inhibited significantly after EYA3 knockdown (KD), since the intensity of γH2AX in EYA3 KD cells with a combination treatment of Lag A and DXR increased obviously compared with that in NT control group. Moreover, to further confirm this effect, Western blot was conducted using the same conditions as for imaging. As expected, the expression level of γH2AX in the cells treated with Lag A and DXR combination was elevated in EYA3 KD cells compared to that of NT control cells (Figure 12B). Both results substantiate that EYA3 silencing rescues the effect of Lag A in inhibiting the formation of DNA damage repair foci after treatment with DXR.

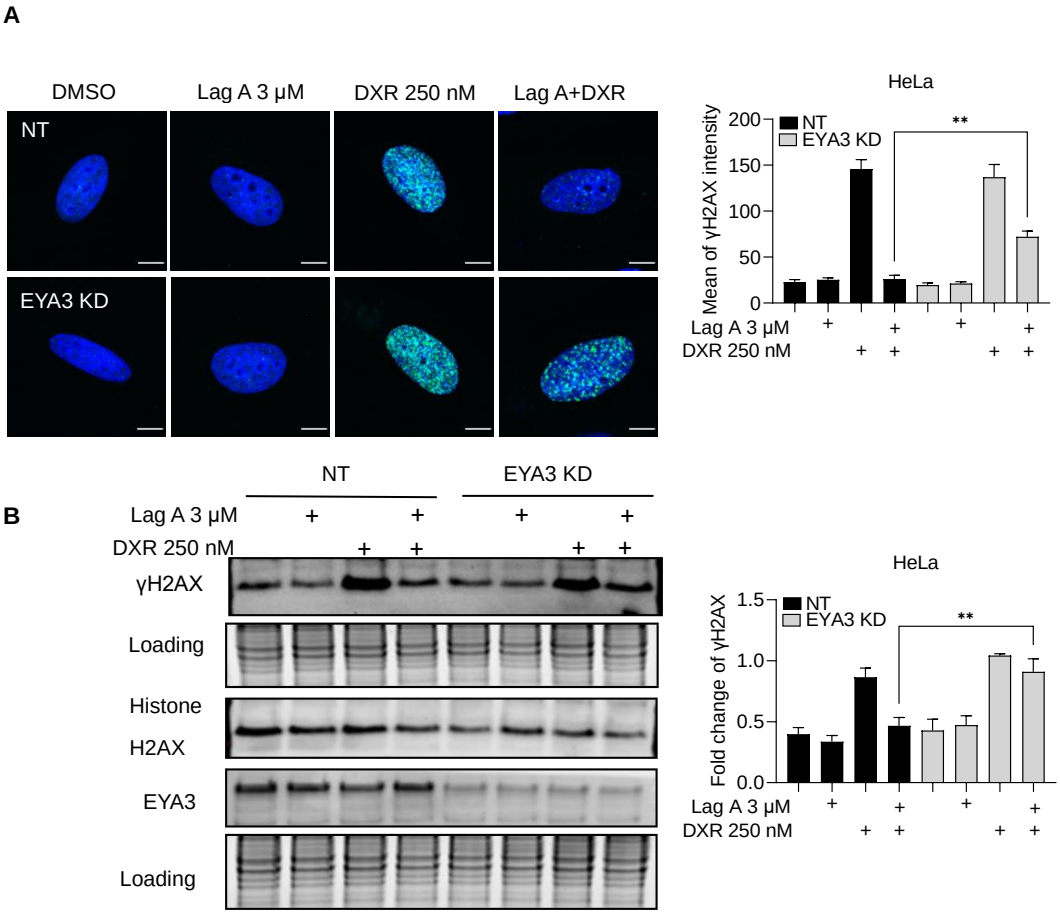

Figure 12. Lag A inhibits formation of DNA damage repair foci after treatment with doxorubicin via interaction with EYA3. (A) Left: As in Figure 11A, except HeLa cells were transfected with NT siRNA or EYA3 siRNA for 24 h prior to indicated compounds treatment. Right: Quantification of γH2AX fluorescence intensity using ImageJ. At least 70 cells were collected in each group for quantitative analysis and data are presented as means ± SEM, n=3, one-way ANOVA, Tukey's test, **P<0.002. Scale bar: 10 μm. (B) Left: As in Figure 11C, except HeLa cells were transfected with NT

siRNA or EYA3 siRNA for 24 h prior to indicated compounds treatment. Right: Immunoblot quantification of γH2AX expression level normalized to Histone H2AX using ImageJ. (Data are presented as means ± SEM, n=3, one-way ANOVA, Tukey's test, **P<0.002)

4.5 Summary

Lagunamide A is a biologically active natural compound with a yet unidentified cellular target. With an affinity-based approach, we failed to identify a target protein. In contrast, by using thermal proteome profiling, we found the proteins EYA3, SMC1A and NDC80 as putative targets. Genetic depletion of EYA3 showed little effect of Lag A on cancer cell proliferation and apoptosis. However, EYA3 turned out to be important for DNA damage repair, and incubation with Lag A sensitized tumor cells to treatment with the drug doxorubicin. This work demonstrates that depending on the target protein different target identification techniques are needed. Furthermore, we show that Lagunamide A might serve as a chemosensitizing agent in the tumor context.

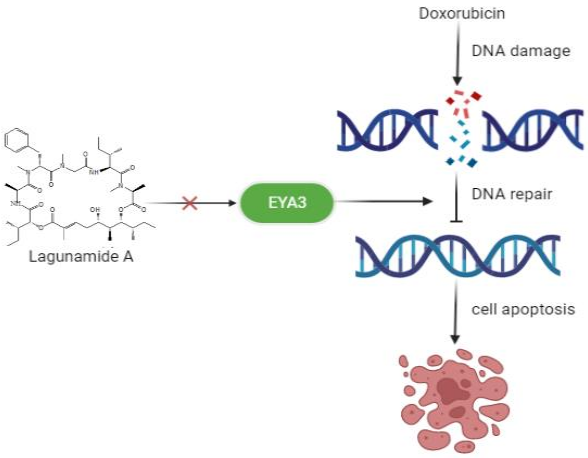

Figure 13. Lagunamide A project summary

RESULTS PART II
---NEOCARZILIN A

5. Results-Part II

5.1 Chemical proteomics identify BST-2 as a cellular target of Neocarzilin A.

Neocarzilin A has been found to show a cytotoxic activity against K562 chronic myelogenous leukemia as early as 1992. The previous work in our lab revealed that NCA had potential inhibitory effects on cell proliferation and cell migration and to uncover the potential targets of NCA, with MS-based activity-based protein profiling (ABPP), we identified that VAT-1 was the anti-migratory target of NCA[24]. However, we found that VAT-1 knock-out had no significant influence on the effect of anti-proliferative effect of NCA on HEK293 FT cells. It indicated that NCA inhibited cell proliferation via other targets.

With the question to know the anti-proliferative target(s) of NCA, target identification and validation experiments were performed by Josef Braun (Group of Prof. Sieber, Department of Chemistry, Technical University of Munich, Germany) using MS-based activity-based protein profiling (ABPP). For ABPP experiments, the activity-based probe NC-4 was synthesized according to Supplementary Scheme 1 (Figure 14A). ABPP result revealed the Bone Marrow Stromal Antigen 2 (BST-2) as most significant and highly enriched target apart from VAT-1 (Figure 14B). Competitive studies with an excess of NCA over NC-4 further confirmed the result. The enrichment of BST-2 was highly decreased with NCA treatment and it indicated that the natural compound NCA and the probe NC-4 competed for the same target (Figure 14C). In conclusion, BST-2 seems to be a promising target of NCA.

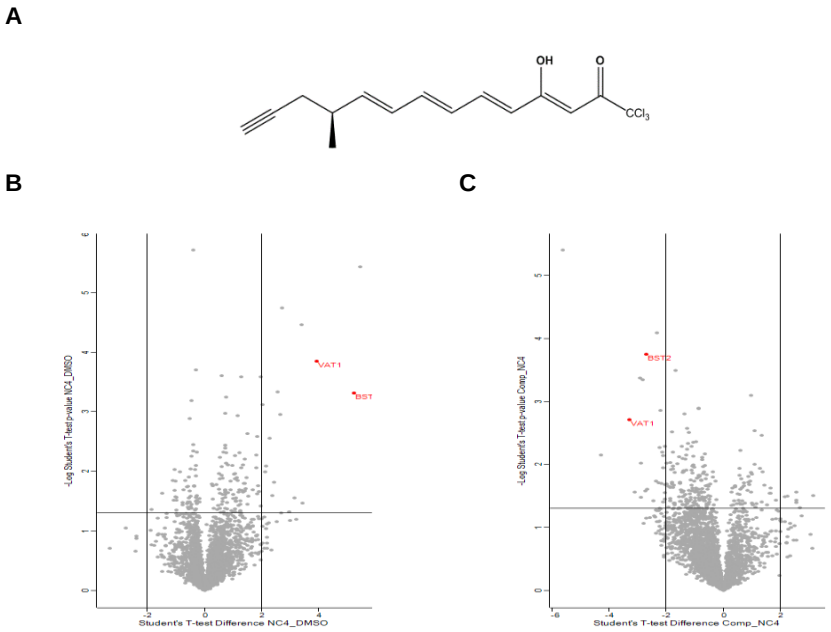

Figure 14. Identification of BST-2 as a cellular target protein of NCA. (A) The structure of ABPP probe NC-4. (B) Volcano plot of in situ ABPP experiment with 250 nM NC-4. (C) Volcano plot of in situ competitive ABPP experiment with 250 nM NC-4 and 25 µM NCA. (B, C) Hits (log_2(enrichment) > 2, p-value < 0.05) are highlighted and the protein with the highest enrichment factor (BST-2 and VAT-1) are shown in red. Proteins that were significantly enriched in NC-4 treated cells in comparison to DMSO control treated cells are listed in Supplementary Table 2 in the Appendix. Experiments were performed by Josef Braun (Group of Prof. Sieber, Department of Chemistry, Technical University of Munich, Germany).

5.2 BST-2 affects the anti-proliferative effect of NCA.

To investigate whether BST-2 is the anti-proliferative target of NCA, genetic knockdown (KD) was used. The successful transfection of BST-2 siRNA in HeLa cells were detected using Western blot (Figure 15A). BST-2 KD cells and NT control cells were stimulated with NCA or DMSO for 72 h and the crystal violet assay was performed. First, we discovered that BST-2 KD did not influence cell proliferation compared to the NT control group (Figure 15B). Based on this result, the inhibition curve of BST-2 KD cells shifted to the right compared to that of NT control group and it indicated that the anti-proliferative effect of NCA was weakened in the absence of BST-2 (Figure 15C). Due to the incomplete BST-2 KD, the remaining BST-2 protein bound to NCA, which prevented us from detecting the rescue effect, and this prompted us to construct a BST-2 knockout cell line.

Moreover, BST-2 over-expression experiment was performed to check whether BST-2 is the anti-proliferative effect of NCA. First, the successful transfection of

BST-2 plasmid was detected using Western blot (Figure 15D). BST-2 over-expression (OE) cells and p-base control (ctl) cells were treated with NCA or DMSO for 72 h and crystal violet assay was performed. The inhibition curve of BST-2 OE cells shifted to the left compared to ctl group and it indicated that BST-2 OE increased cell sensitivity to NCA treatment, while BST-2 OE did not influence cell proliferation (Figure 15E and 15F).

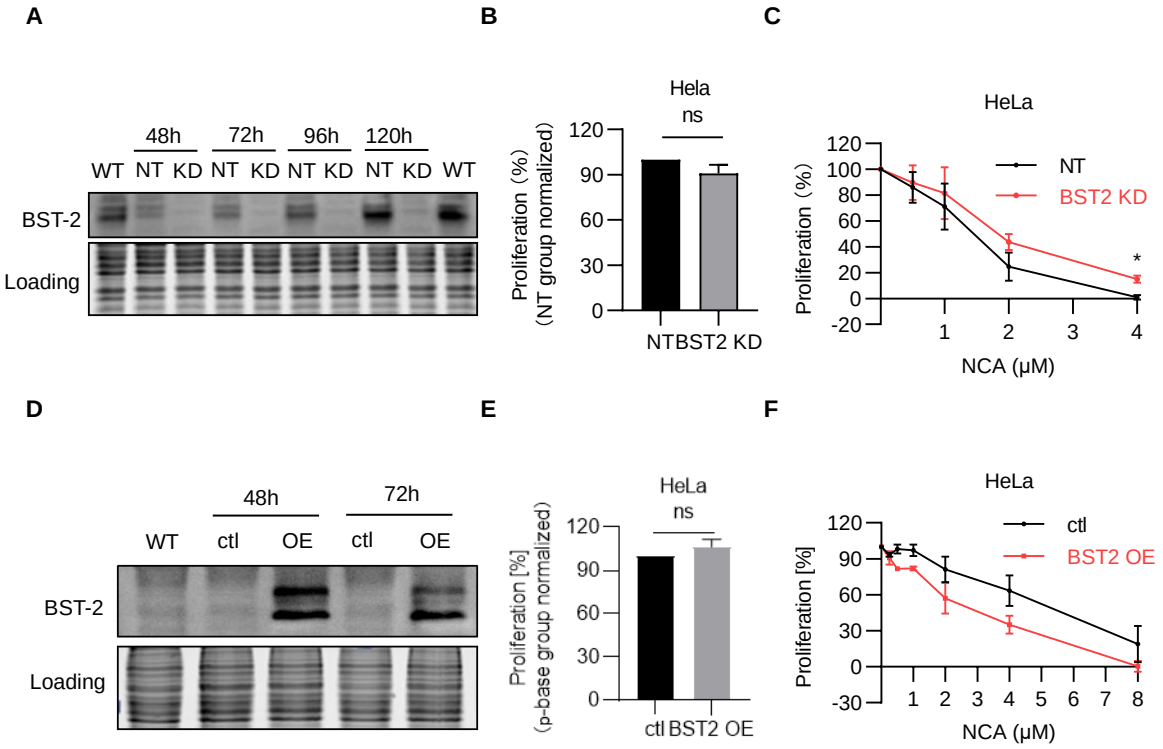

Figure 15. BST-2 regulates the anti-proliferative effect of NCA. (A) Western blot of BST-2 protein levels in non-targeting (NT) and BST-2 siRNA (knockdown, KD) HeLa after 48, 72, 96 and 120 h transfection. (B) Cell proliferation of NT and BST-2 KD HeLa cells determined by crystal violet staining assay after 72 h. (C) Anti-proliferative effect of NCA in NT and BST-2 KD HeLa cells measured by crystal violet staining assay. Cells were treated with indicated concentrations of NCA for 72 h. Data are presented as means ± SEM, n=3, one-way ANOVA, Dunnett's test, *p<0.033. (D) Western blot of BST-2 protein levels in empty plasmid (ctl) and BST-2 plasmid over-expression (OE) HeLa after 48 and 72 h transfection. (E) Cell proliferation of ctl and BST-2 OE transfected HeLa cells determined by crystal violet staining assay after 72 h. (F) Anti-proliferative effect of NCA in ctl and BST-2 OE transfected HeLa cells measured by crystal violet staining assay after 72 h. Data are presented as means ± SEM, n=3.

5.3 Generation and validation of a BST-2 knockout cell line.

To further investigate whether BST-2 is the anti-proliferative target of NCA, BST-2 was knocked out using the CRISPR-Cas9 system in HeLa cells and two different gRNAs targeting BST-2 gene were designed and then limited dilution was performed to generate BST-2 knockout (KO) cells. Successful deletion of BST-2 was determined

by Western blot and Flow cytometry. Firstly, Western blot was performed to compare the BST-2 expression level in wild type (WT) cells and KO clones and these data showed that no BST-2 band could be detected in all of the BST-2 KO candidates (Figure 16A). To further verify BST-2 KO clones, BST-2 surface level was investigated with Flow cytometry and BST-2 surface levels were significantly decreased to level consistent with negative control cells (isotype) (Figure 16B). In addition, BST-2 KO clones were identified by Josef Braun (Group of Prof. Sieber, Department of Chemistry, Technical University of Munich, Germany) to further confirm the KO cells using full proteome. In accordance with Western blot and Flow cytometry results, no BST-2 protein could be detected compared to WT cells by the MS in all BST-2 KO clones (Figure 16C). In summary, BST-2 knockout clones were successfully generated to study whether BST-2 is the anti-proliferative target of NCA.

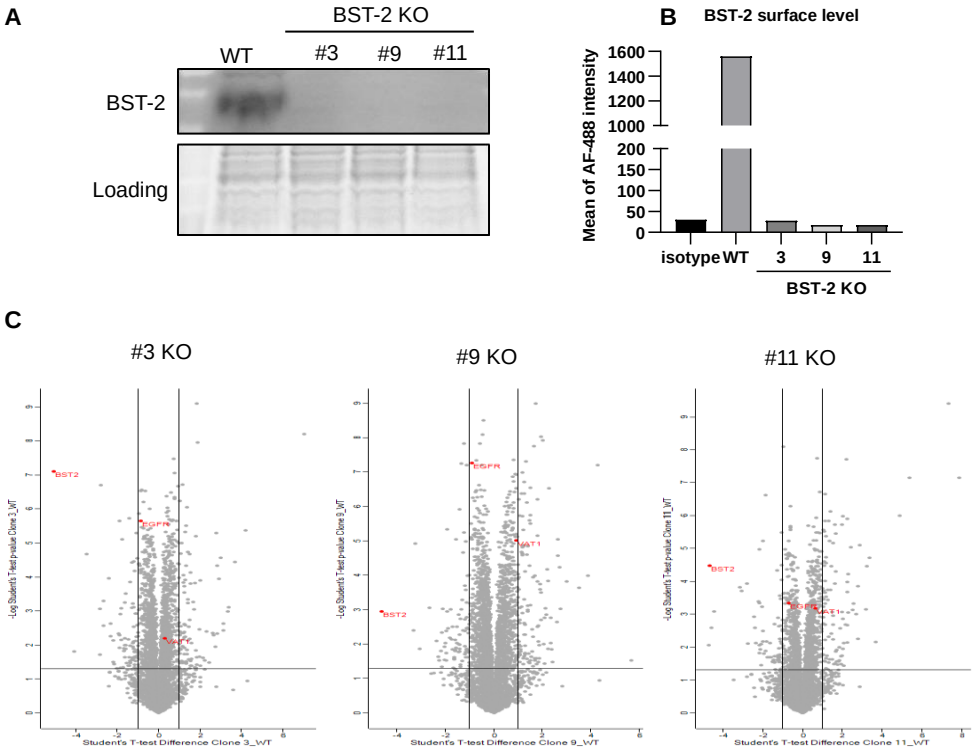

Figure 16. Generation and validation of a BST-2 knockout cell line. (A) Western blot of BST-2 protein levels in HeLa BST-2 KO clones generated via the CRISPR-Cas9 method. (B) BST-2 surface levels in HeLa BST-2 KO clones detected by Flow cytometry. (C) Successful knockout of BST-2 was confirmed by measuring BST-2 protein enrichment using Full proteomics by Josef Braun (Group of Prof. Sieber, Department of Chemistry, Technical University of Munich, Germany).

5.4 BST-2 is the anti-proliferative target of NCA.

Next, to investigate the role of BST-2 in the anti-proliferative effect of NCA, we randomly selected three BST-2 knockout (KO) clones with the same morphology as the WT control cells and crystal violet assay was performed. First of all, BST-2 KO cells proliferated slower than WT cells (Figure 17A), although no significant difference could be detected and it may due to that some compensation pathways were activated. Based on this, the anti-proliferative effect of NCA in BST-2 KO and WT cells were detected. Cells were treated with different concentrations of NCA and incubated for 72 h, results showed that the proliferation curve of all three BST-2 KO cells shifted to the right side compared to that in WT cells, especially at 1 μM (Figure 17B). To clearly illustrate the difference, 1 μM was selected and we found the viable cells of all three BST-2 KO cells increased significantly compared to the value in WT group (Figure 17C). These results demonstrate that BST-2 KO antagonizes the anti-proliferative effect of NCA and BST-2 is the promising anti-proliferation target of NCA.

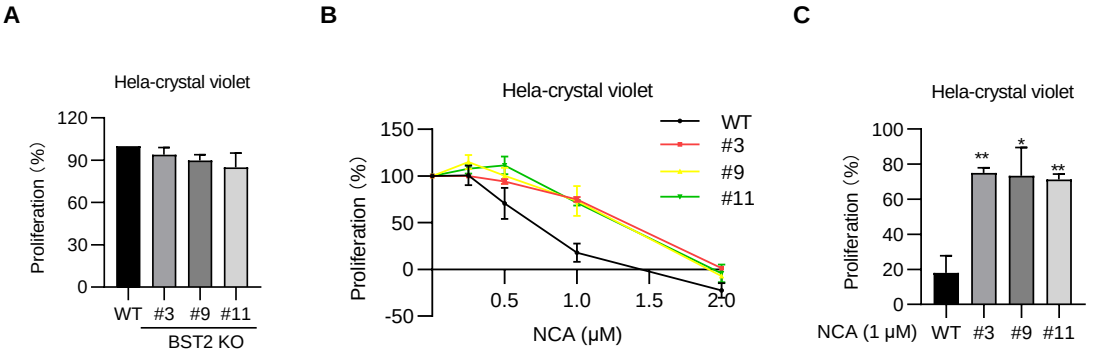

Figure 17. BST-2 KO strongly affects the anti-proliferative effect of NCA. (A) Cell proliferation of WT and BST-2 KO cells determined by crystal violet staining assay after 72 h. (B) Anti-proliferative effect of NCA in WT and BST-2 KO cells measured by crystal violet staining assay. Cells were treated with indicated concentrations of NCA for 72 h. (C) Proliferation of WT and BST-2 KO cells with 1 μM NCA treatment. Data are presented as means ± SEM, n=3, one-way ANOVA, Dunnett's test, *p<0.033, **P<0.002.

To further confirm the specificity of BST-2, rescue experiments were performed to know the effect is caused by BST-2, not others. Then we used the BST-2 plasmid to re-express BST-2 protein in BST-2 KO cells in order to rescue the knockout phenotype. The successful transfection of BST-2 plasmid in BST-2 KO cells were

detected using Western blot (Figure 18A) and the BST-2 expression level in KO cell line that was re-expressed BST-2 raised to a comparable extent as observed with WT control cells. Next, different concentrations of NCA were used to treat with WT cells, BST-2 KO cells and BST-2 KO cells with BST-2 reconstitution and crystal violet assay was used to detect cell proliferation. Similarly, the anti-proliferative effect of NCA was weaken in KO cells which was consistent with our previous data, however, the proliferation curve of KO cells with BST-2 reconstitution shifted to the left side and nearly coincided with the curve of the WT control cells and it indicated that BST-2 reconstitution fully blocked the knockout effect (Figure 18B). In summary, these results prove that BST-2 is the anti-proliferative target of NCA.

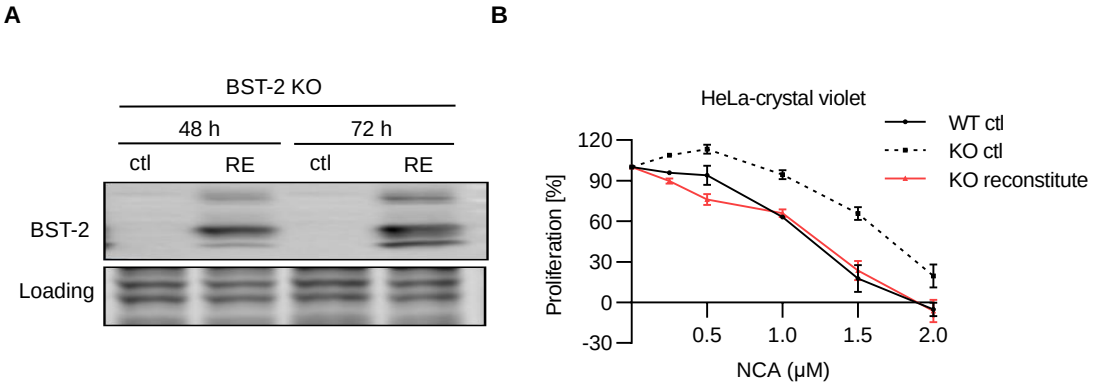

Figure 18. BST-2 reconstitution rescues the effect of BST-2 KO. (A) Western blot of BST-2 protein levels in empty plasmid (ctl) and BST-2 plasmid reconstitution (RE) in HeLa BST-2 KO cells after 48 and 72 h transfection. (B) Anti-proliferative effect of NCA in WT ctl cells, BST-2 KO ctl cells and BST-2 KO reconstitution cells was measured by crystal violet staining assay. Cells were treated with indicated concentrations of NCA for 72 h.

5.5 Mechanistic study

5.5.1 NCA promotes BST-2 degradation via the lysosomal pathway without disturbing BST-2 distribution.

After having proved that BST-2 is the anti-proliferative target of NCA, we aimed at investigating the effect of NCA on BST-2. Interestingly, we found that BST-2 protein level decreased significantly in a dose-dependent manner when subtoxic concentrations of NCA were used to treat HeLa cells for 24 h and only with 5 μM NCA, BST-2 protein levels dropped to 50% of that in DMSO control group (Figure 19A and

19B). In addition, we were curious about whether NCA influenced BST-2 protein level within shorter treatment times. However, BST-2 protein level remained unchanged upon high concentration NCA treatment in 6 h (Figure 19C). Meanwhile, full proteomics analysis confirmed the effect of NCA on BST-2 protein down-regulation after 24 h incubation time (Figure 19D). It demonstrates that NCA significantly decreases BST-2 protein level after 24 h treatment.

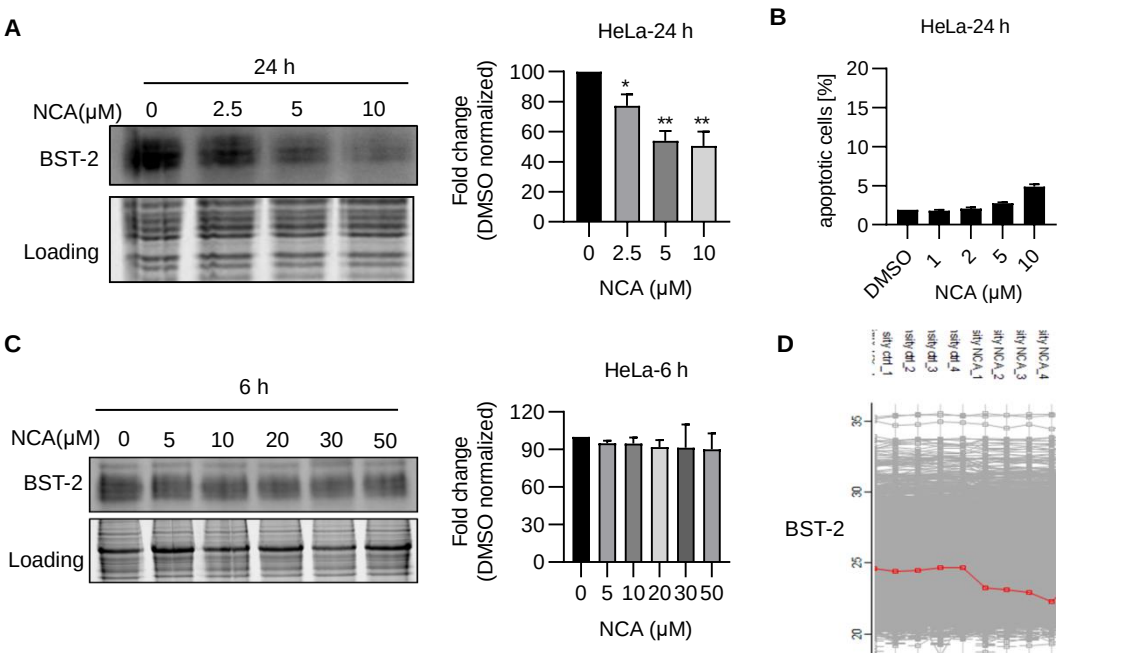

Figure 19. NCA decreases BST-2 protein expression after 24 h. (A) Western blot analysis of BST-2 protein level in HeLa cells treated with different concentrations of NCA for 24 h. Representative blots of three independent experiments are shown. Amount of BST-2 was normalized to loading control and results were normalized to the DMSO control. Data are presented as means ± SEM, n=3, one-way ANOVA, Dunnett's test, *p<0.033, **P<0.002. (B) Concentrations of NCA were subtoxic. HeLa cells were treated with indicated NCA and cell apoptosis was conducted by Nicoletti assay and flow cytometry. (C) Western blot analysis of BST-2 protein level in HeLa cells treated with different concentrations of NCA for 6 h. Representative blots of three independent experiments are shown. Amount of BST-2 was normalized to loading control and results were normalized to the DMSO control. (D) Full proteomics analysis of BST-2 protein level in HeLa cells with 5 μM NCA treatment was done by Josef Braun (Group of Prof. Sieber, Department of Chemistry, Technical University of Munich, Germany).

Next, we endeavoured to characterize the effect in detail to know how NCA regulated BST-2 protein level after 24 h treatment. As we know, there are three major ways to regulate protein levels: the first way is through the mRNA level, the second way is through protein degradation and the last way is through protein synthesis regulation. Firstly, to know whether NCA affected BST-2 protein level via mRNA regulation,

qPCR experiment was performed to detect the effect of NCA on BST-2 mRNA level. BST-2 mRNA level did not change with the NCA treatment compared to that of the DMSO control (Supplementary Figure 4) and it suggested NCA did not influence the BST-2 expression via mRNA level, and the decrease in BST-2 level was occurring at the protein level. Based on this result, we further investigated whether NCA down-regulated BST-2 protein level through promoting protein degradation. As reported in the literature[109], cells use proteasome pathway and lysosomal proteolysis (including autophagy) to regulate protein degradation. To know whether NCA affected BST-2 protein level through the proteasome pathway, MG132, a widely-used proteasome inhibitor, was used but it failed to rescue BST-2 protein expression to the level of control by applying combination treatment of NCA and MG132 (Figure 20B). Meanwhile, we explored whether NCA regulated BST-2 protein level through the lysosomal pathway. Two different lysosomal inhibitors, Bafilomycin A1 (BFA) and Chloroquine (CQ) were used. Surprisingly, BST-2 protein level was rescued to the level of control in the presence of BFA or CQ, especially with BFA treatment, although BFA or CQ alone caused an increase in total BST-2 protein (Figure 20A). Consequently, NCA influenced BST-2 protein expression via the lysosomal degradation pathway. Nowadays, many researchers acknowledge that targeted protein degradation technology has evolved a brand-new therapeutic modality from an innovative drug discovery perspective.

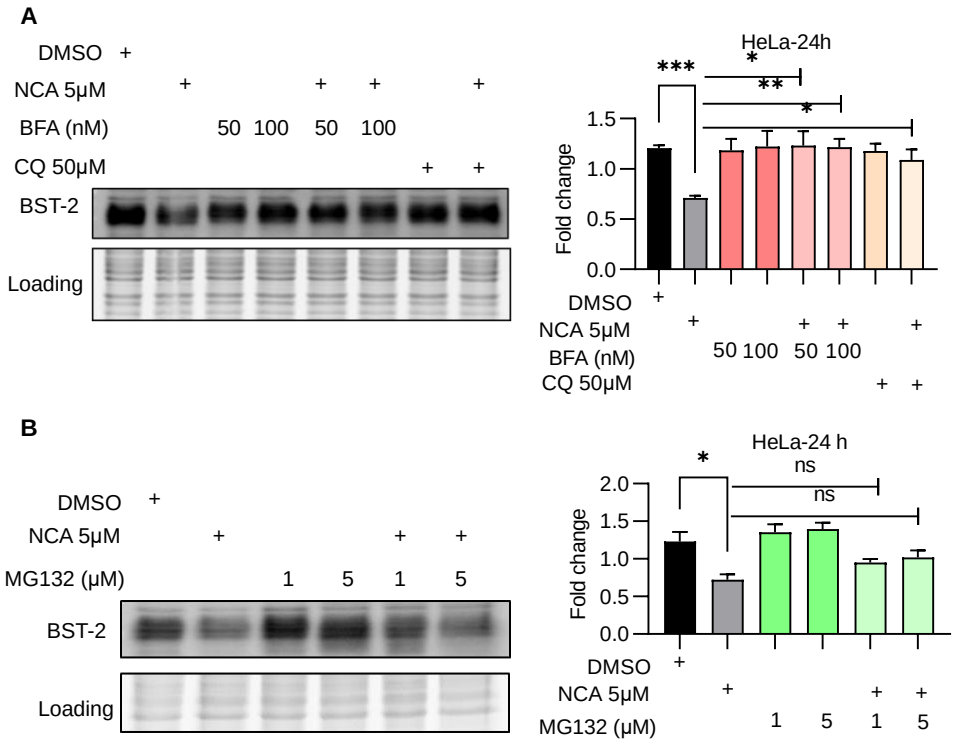

Figure 20. NCA promotes BST-2 degradation via lysosomal pathway. (A) Western blot analysis of BST-2 protein level in HeLa cells with indicated treatment. HeLa cells were pre-treated with BFA or CQ for 1 h before NCA treatment for 24 h. Representative blots of three independent experiments are shown. Amount of BST-2 was normalized to loading control and data are presented as means ± SEM, n=3, one-way ANOVA, Tukey's test, *p<0.033, **P<0.002, ***P<0.001. (B) Western blot analysis of BST-2 protein level in HeLa cells with indicated treatment. HeLa cells were pre-treated with MG132 for 1 h before NCA treatment for 24 h. Representative blots of three independent experiments are shown. Amount of BST-2 was normalized to loading control and data are presented as means ± SEM, n=3, one-way ANOVA, Tukey's test, $^{ns}p>0.12$, *p<0.033.

Since BST-2, as a membrane protein, mainly plays its biological role in the cell membrane, detecting BST-2 surface level is important to ascertain the effect of NCA on the function of BST-2 protein. Therefore, we investigated the effect of NCA on BST-2 surface level using Flow cytometry. Similar to Western blot data, NCA down-regulated BST-2 surface level after 24 h treatment compared to that of DMSO control, while within 6 h, no difference on the BST-2 surface level was found (Figure 21A). Based on this result, we further detected BST-2 surface level with different concentrations of NCA at 24 h and BST-2 surface levels were reduced in a dose-dependent manner (Figure 21B).

Next, we investigated the effect of NCA on BST-2 distribution and fluorescence

intensity with or without cell membrane permeabilization. 10 μM NCA and 24 h were chosen as treatment conditions. In the DMSO control, the green fluorescence conjugated BST-2 was detected throughout the cytoplasm, especially accumulation around the nuclear (Figure 21C). Studies in the literature suggested that BST-2 distributes in Golgi apparatus, cytoplasmic and membrane localization[110]. As expected, upon NCA treatment, a significant drop in BST-2 fluorescence intensity was detected when compared to that of the DMSO control group (Figure 21C and 21 D). However, BST-2 distribution did not change upon NCA treatment with or without permeabilization.

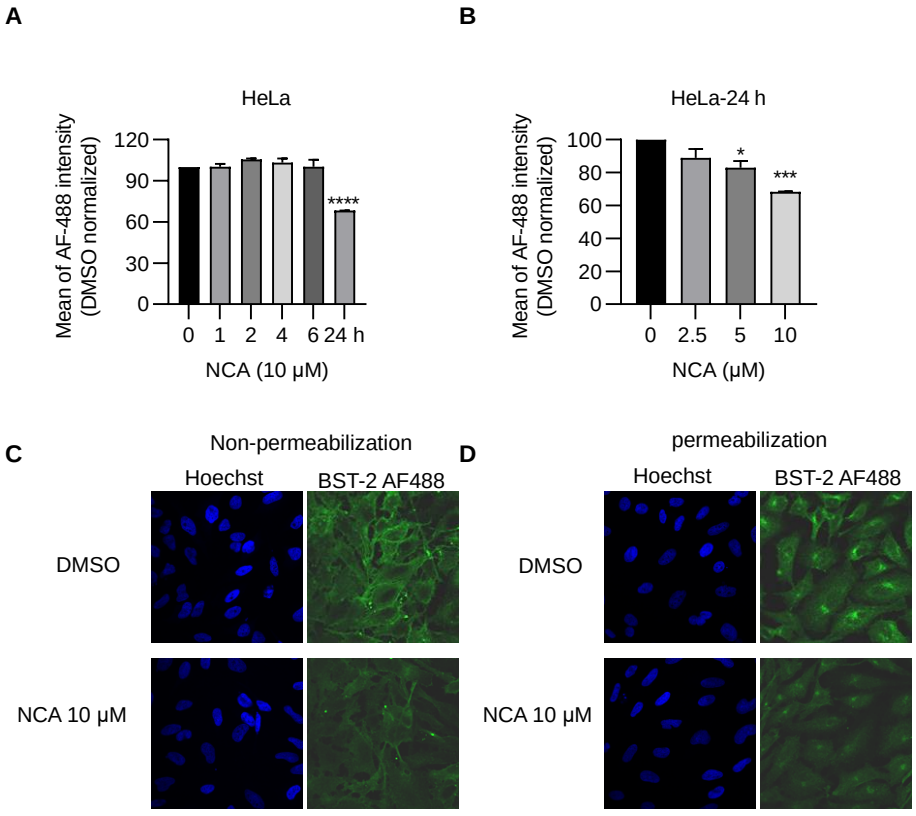

Figure 21. NCA decreases BST-2 surface level and the fluorescence intensity of BST-2 without affecting BST-2 distribution. (A) BST-2 surface levels analysis of HeLa cells with NCA treatment. HeLa cells were treated with 10 μM NCA for indicated time points and BST-2 surface levels were determined by Flow cytometry. Data are presented as means ± SEM, n=3, one-way ANOVA, Dunnett's test, ****P<0.0001. (B) BST-2 surface levels analysis of HeLa cells with indicated concentrations of NCA for 24 h. Data are presented as means ± SEM, n=3, one-way ANOVA, Dunnett's test, *p<0.033, ***P<0.001. (C) Immunofluorescence staining of BST-2 (green) without permeabilization in HeLa cells stimulated with NCA or DMSO as indicated. Nuclei were stained with Hoechst 33342 (Blue). Representative images out of three independent experiments are shown. (D) Immunofluorescence staining of BST-2 (green) with permeabilization in HeLa cells stimulated with NCA or DMSO as indicated. Nuclei were stained with Hoechst 33342 (Blue). Representative images out of three independent experiments are shown.

5.5.2 BST-2 and NCA influence the EGFR signaling pathway and dynamics.

As outlined in chapter 5.5.1, NCA decreased BST-2 protein levels via the lysosomal pathway, and for a more in-depth study of the mechanisms, we investigated how targeting BST-2 degradation acts as the anti-proliferative target of NCA. Recently Xiaochun Wan[101] suggested the relationship between BST-2 and EGFR signaling pathway and they found that CD317 (also called BST-2), a surface molecule with a unique topology, activated EGFR in hepatocellular carcinoma (HCC) cells by regulating its localization on the plasma membrane and then initiated downstream signaling pathways, including the Ras–Raf–MEK–ERK and JAK–STAT pathways. To confirm the findings in HeLa cells directly, we first compared the EGFR signaling pathway and its downstream signaling pathway between WT and BST-2 KO cells. We observed that BST-2 KO decreased the phosphorylation of EGFR at Tyr1068 and down-regulated the activation of STAT3 in HeLa cells with an enhancement of the activation of ERK (Figure 22A and 22B). The difference in the activation of ERK may due to different cell lines and the methods to achieve BST-2 down-regulation. Our results demonstrate that BST-2 indeed regulates the EGFR signaling pathway in HeLa cells.

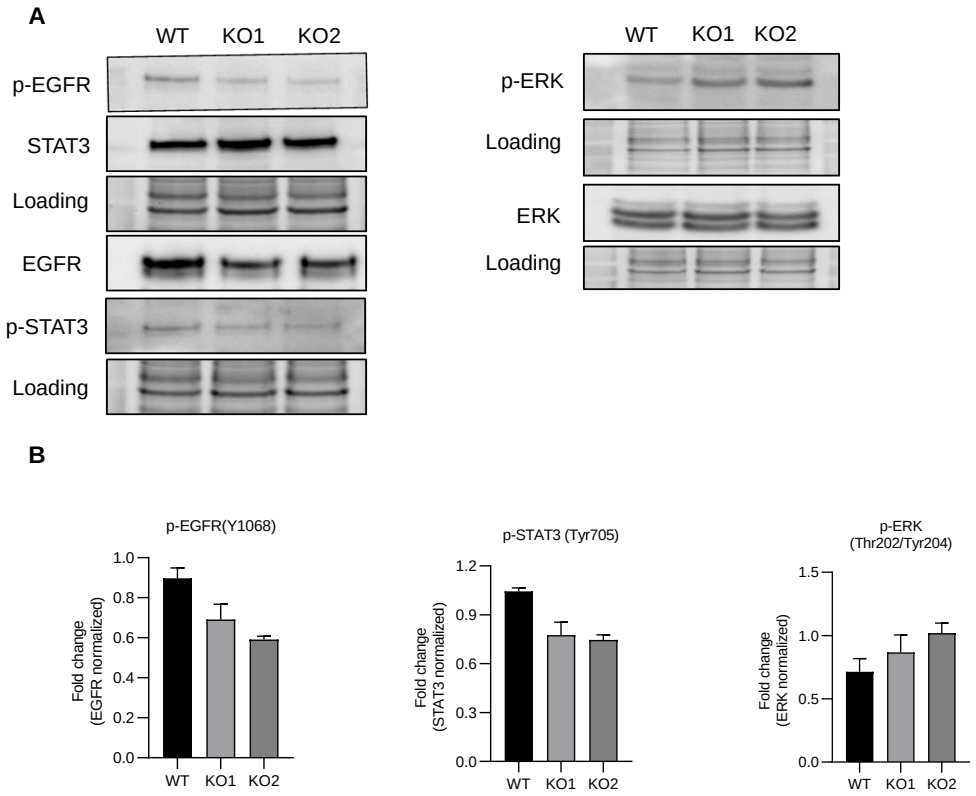

Figure 22. BST-2 KO influences the EGFR signaling pathway. (A) Western blot analysis of EGFR, STAT3, ERK, p-STAT3, p-EGFR and p-ERK protein levels in WT and BST-2 KO cells. Representative blots of three independent experiments are shown. (B) Bar graphs show the mean ± SEM of three independent experiments and the amount of p-EGFR, p-STAT3 and p-ERK were normalized to EGFR, STAT3 or ERK respectively.

Since NCA decreased BST-2 protein level and BST-2 is the anti-proliferative target of NCA, next we investigated whether NCA led to a reduction in EGFR phosphorylation events or EGFR downstream signaling pathways. As expected, the phosphorylation of EGFR was decreased significantly upon NCA treatment and a decrease in phosphorylation of STAT3 was detected in a dose-dependent manner (Figure 23A and 23B), although an increase in phosphorylation of ERK was observed (data not shown), which was consistent with that of BST-2 KO. Collectively, these data show that NCA decreases BST-2 protein level and then causes down-regulation in EGFR signaling pathway.

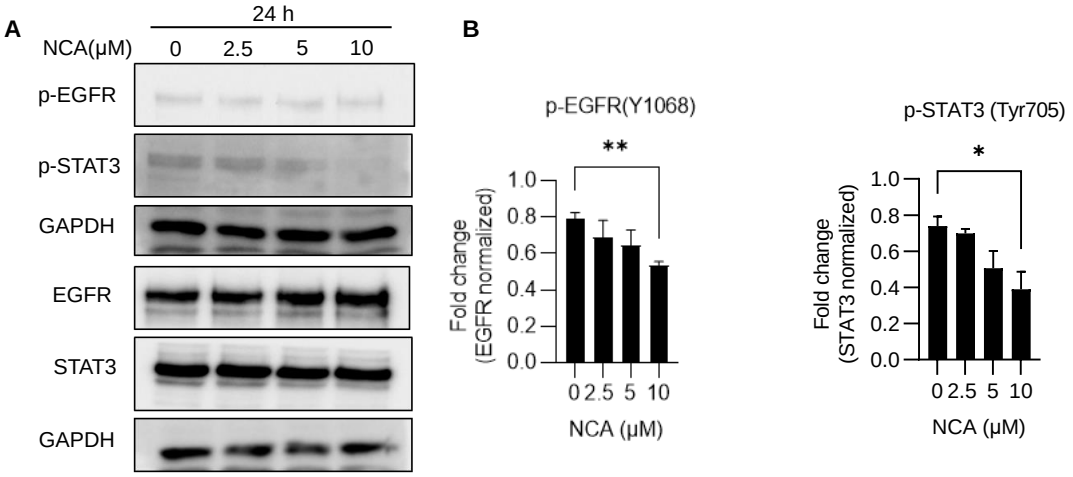

Figure 23. NCA affects the EGFR signaling pathway. (A) Western blot analysis of EGFR, STAT3, p-STAT3 and p-EGFR protein levels in HeLa cells with indicated concentrations of NCA treatment for 24 h. Representative blots of three independent experiments are shown. (B) Bar graphs show the mean ± SEM of three independent experiments and the amount of p-EGFR and p-STAT3 were normalized to EGFR or STAT3 respectively. One-way ANOVA, Dunnett's test, *p<0.033, **P<0.002.

Since EGFR signaling pathway is important for NCA and BST-2 to regulate cell proliferation, we focused on the EGFR protein and the fluorescence recovery after photobleaching (FRAP) experiment was performed to visualize the lateral mobility and dynamics of GFP-tagged EGFR in living cells. Firstly, to know how BST-2 regulated EGFR protein lateral mobility and dynamics, we transfected WT cells and BST-2 KO cells with a plasmid that expressed GFP tagged EGFR respectively and compared the FRAP efficiency between WT and BST-2 KO cells after transfection. Interestingly, the calculated mobile fraction R of two BST-2 KO cells were increased compared with that of WT cells (Figure 24A). It indicated that BST-2 KO accelerated the lateral mobility and dynamics of EGFR protein. Next, to detect the effect of NCA on the EGFR protein dynamics and activity within a single living cell, cells were treated with NCA for 24 h after transfection with the GFP tagged EGFR plasmid and then FRAP experiment was performed. As expected, an increase on the mobile fraction R was detected after NCA treatment compared to that of DMSO control, although the effect was not as strong as that of BST-2 KO (Figure 24B). Collectively, these data indicate that both BST-2 and NCA regulate EGFR dynamics.

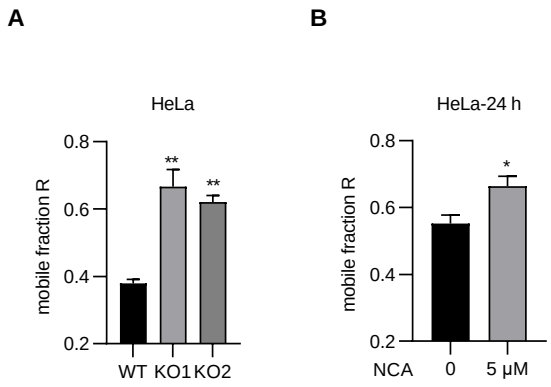

Figure 24. NCA and BST-2 KO promote the lateral mobility and dynamics of EGFR protein. (A) The lateral mobility and dynamics of EGFR protein were detected in WT and BST-2 KO clones using FRAP experiment. Bar graph shows the mean ± SEM of three independent experiments, one-way ANOVA, Dunnett's test, **P<0.002. (B) The lateral mobility and dynamics of EGFR protein were detected in DMSO or NCA treated HeLa cells using FRAP experiment. Bar graph shows the mean ± SEM, n=3, unpaired t-test with Welch's correction, *p<0.033.

5.5.3 NCA affects EGFR activation through lipid rafts.

To better know how NCA affects EGFR protein and EGFR signaling pathway, since the activation of EGFR is regulated by its localization to lipid rafts and Guizhong Zhang revealed that the activation of EGFR was controlled via BST-2-mediated release from the lipid rafts, which facilitated the activation of EGFR and the initiation of downstream signaling pathways[101], we then investigated whether NCA affected the raft versus non-raft distribution of EGFR. Using a fluorescently-tagged choleratoxin B subunit (CTB) that specifically labels lipid rafts, we observed that NCA-treated HeLa cells exhibited high levels of co-localization of EGFR with lipid rafts, characterized by an increased coefficient value (Pearson R value) between EGFR and lipid rafts staining (Figure 25A and 25B). Taken together, NCA promoted the colocalization between lipid rafts and EGFR, which fits our hypothesis that NCA decreases BST-2 protein level and disturbs the activation of EGFR via lipid rafts.

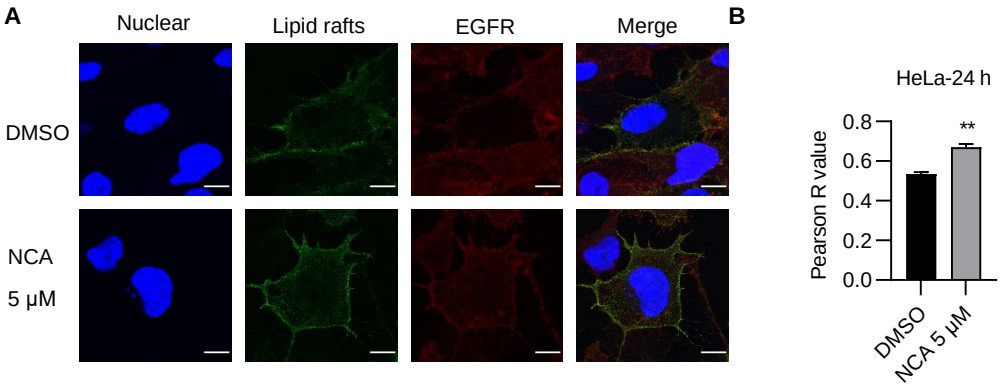

Figure 25. NCA increases the co-localization of EGFR with lipid rafts. (A) HeLa cells treated with DMSO or NCA were immunostained for EGFR (red), lipid rafts (green), and nuclear (Hoechst 33342, blue). Shown are representative fluorescence images. Scale bar: 10 µm. (B) EGFR-lipid rafts colocalization plot, and Pearson's correlation coefficient (R) (right; mean ± SEM for at least 60 cells). Unpaired t-test with Welch's correction, **P<0.01.

5.6 Summary

Neocarzilin A is a biologically active natural compound and our previous study identified VAT-1 protein as NCA's anti-migratory target; nevertheless, NCA also has a significant anti-proliferative impact on cancer cells, but the responsible target for anti-proliferative effect still needs to be identified. The main finding of this work is the identification of NCA as an inhibitor of cancer cell proliferation by interacting with BST-2 protein, which was identified as cellular target of NCA via proteomics-based ABPP experiments. In summary, NCA strongly suppressed cell growth *in vitro*, and we identified the protein BST-2 as a possible target using an affinity-based method. Genetic knockdown or depletion of BST-2 showed strong effect of NCA on cancer cell proliferation. Subsequent rescue experiments with BST-2 over-expression or reconstitution verified the specificity of BST-2's function in the anti-proliferative effect of NCA. In terms of the anti-proliferative mechanism of BST-2 or NCA, we were able to attribute the strong anti-proliferative effect of BST-2 to EGFR signaling pathway and NCA exhibited consistent effects as well. Facilitating these results, FRAP assay and lipid rafts staining confirmed the link between BST-2 or NCA and lipid rafts. This work demonstrates that NCA targets cancer cell proliferation via binding to the BST-2 and BST-2 might serve as a potent target for cancer therapy.

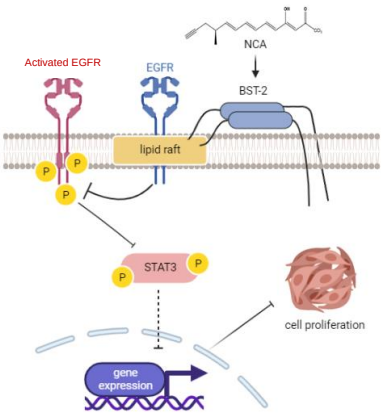

Figure 26. Neocarzilin A project summary

DISCUSSION

6. Discussion

6.1 Part I Identification of EYA3 as a novel target for the natural compound Lagunamide A

6.1.1 Lagunamide A as a promising anticancer compound

Previous studies only focused on its structure and anti-tumor effects of Lag A[18, 21], with no potential targets being investigated or proposed. Since the natural compound Aurilide shares many structural features of Lag A, and a mitochondrial target (prohibitin) has been identified for this compound in an affinity-based approach[19], we also started by investigating viability and mitochondria-based effects of Lag A.

To gain more insight into this interesting natural compound class, we performed detailed analysis of their antitumor activities against the structure and structure-activity relationship (SAR) was performed and recognized them as antitumor agents showing the most prominent effects on inhibition of cell proliferation and apoptosis. Strikingly, the Lag A analogues showed diverse potency depending on their chemical structure and stereochemistry. Comparison of the effects of Lag A, the activities of OA412-1 and OA469-1 dramatically decreased, which revealed that changes in the parent nucleus of the structure of Lag A resulted in reduced anti-proliferative and anti-apoptotic effects (Supplementary Figure 1). Moreover, single modification of function group on the basic structure of Lag A did not contribute to significant change on the anti-tumor effect of Lag A. This study would guide the further structure optimization.

6.1.2 Chemical proteomics as powerful tools in the target identification of Lagunamide A

Characterizing novel natural compounds, their targets and their mode of action is one of the most challenging tasks in drug discovery, especially in the context of cancer therapy[111]. Compound supply and complicated total synthesis are the main

bottlenecks for this kind of research. Proteomics approaches have made target identification much more feasible and we have successfully applied different techniques to identify targets of natural compounds in recent years[24, 112-116].

We found that Lag A significantly inhibited cell proliferation and promoted cell apoptosis in HeLa and Jurkat cells, with a significant impact on mitochondria function, which was consistent with a previous study[23]. However, affinity-based proteome profiling with Lag A derived probes did not lead to identification of a putative mitochondrial target. Due to synthetic reason we had to place the position for the linker in the Lag A probe at a different place in comparison to the published Aurilide probe [19]. This might explain why we were not able to identify a target protein, though the functional data (e.g. mitochondrial morphology, ATP production, oxygen consumption rate) also clearly point towards a mitochondrial target of Lag A. This also demonstrated that label-based approaches, and the related changes of the structure of the compound of interest severely restrict the applicability of this approach.

Consequently, we used thermal proteome profiling (TPP) as an alternative label-free approach. We identified a number of target candidate proteins, three of which were highly significant: EYA3 (eyes absent homolog 3), SMC1A (Structural maintenance of chromosomes protein 1A) and NDC80 (Kinetochore Protein NDC80 Homolog). EYA3 and SMC1A both play a role in DNA damage repair, while NDC80 organizes and stabilizes microtubule-kinetochore interactions. NDC80 and SMC1A have in common that they are required for proper chromosome segregation[117, 118].

6.1.3 EYA3 as a novel druggable target

In the present work we focused on EYA3 and its role during repair of DNA double strand breaks, since this form of DNA damage repair is crucial to maintain cell survival and genomic stability[119], which are important hallmarks of cancer[120]. Once DNA damage is caused by genetic stress or certain chemotherapeutics (e.g. doxorubicin, which we used), cancer cells will induce the DNA damage repair process, and keep

proliferating and surviving under an adequate DNA damage repair. However, incomplete or inadequate repair potentiates cell death and induces cell apoptosis. γH2AX (phosphorylation of Histone H2AX at Ser319), a marker for DNA damage and repair foci, is widely used to detect this process[107]. Intriguingly, upon Lag A pre-treatment, we barely detected any presence of γH2AX induced by DXR, in contrast to DXR alone. Two alternative explanations are that Lag A either facilitates rapid repair process in that short time, or Lag A completely blocks the repair process. However, our data showed that Lag A and DXR had synergistic effect in promoting apoptosis, which proved that Lag A blocked DXR-induced DNA damage repair and tipped the balance in favor of cell death. In addition, knockdown of EYA3 significantly rescued the formation of γH2AX upon co-treatment of cells with Lag A and DXR.

EYA3 belongs to the Eye Absent (EYA) family, and EYA family members contain the N-terminal transactivation domain and the C-terminal tyrosine phosphatase domain, enabling them to act as transcriptional activators and tyrosine phosphatases[53, 121, 122]. EYA proteins are over-expressed in different cancer cell lines, including breast cancers[31], Ewing sarcoma[54], and lung cancers[123]. Interestingly, we also found that EYA3 KD did as such not affect cell apoptosis and cell proliferation in HeLa cells (data not shown), which is contradictory to a role for EYA3 in cell proliferation as previously reported[31]. This could be due to the cell-type specific effects or the silencing approach.

6.1.4 Future Perspectives

Cancer treatment usually consists of surgery in combination with radiotherapy or chemotherapy. The anticancer activity of most chemotherapy drugs relies on the induction of DNA damage in rapidly cycling tumor cells with inadequate DNA repair. Anthracyclines, for example, cause DNA damage by blocking DNA topoisomerases and producing oxygen radicals. As result, the regulation of DNA repair mechanisms in tumor cells is an important component in how they respond to chemotherapy

treatments. The most common problems encountered while treating cancer patients with chemotherapy are serious toxic side effects caused by a lack of tumor cell specificity and a lack of effectiveness caused by innate or acquired resistance. Specifically, DNA repair Defective tumors (which have a high level of genomic instability) may easily acquire mutations in genes that confer therapeutic resistance. Thus, chemotherapy resistance is an urgent issue for clinical treatment[124, 125].

Based on our results, it would be a promising approach to design and investigate simplified derivatives or fragments of Lag A as lead structures for chemo-sensitizing drug development. With Lag A targeting the DXR-induced DNA damage repair process, we discovered a new druggable step of the DNA damage repair response. By uncovering the molecular mode of action of Lag A, a promising starting point is set to study the basic chemotherapy resistance mechanism and to develop more effective chemo-sensitizing drug based on the Lag A structure.

6.2 Part II Identification of BST-2 as a novel target for the natural product Neocarzilin A

6.2.1 Neocarzilin A as a promising anticancer compound

The Neocarzilins only have received little attention since their discovery in the 1990s by Nozoe et al. Amongst them, Neocarzilin A (NCA) has been shown to have potent cytotoxic effect against the K562 chronic myelogenous leukemia cell line. However, our previous study revealed that NCA exhibited significantly anti-migratory and anti-proliferative effect towards tumor cells, and demonstrated that VAT-1 is the potent target for the inhibiting migration effect of NCA. Moreover, it is worth noting that the Neocarzilins separate themselves from other therapeutically useful natural compounds not only by their powerful anti-migratory and anti-proliferative properties, but also by their comparatively simple chemical structure and production. One of the major obstacles in researching natural compounds is a lack of compound supply, which occurs frequently with natural products, and to overcome this problem, the artificial synthesis technique was developed. Due to the simple chemical structure of NCA and its synthetic accessibility, the natural compound NCA protrudes as interesting object for further research. The natural compound NCA stands out as a fascinating product for future investigation. Besides, our previous work on the structure-activity relationship study indicated that stereochemistry and the trichloromethyl group with its electrophilic character are essential for its biological activity. Taken together, the NCA were found as a promising natural chemical compound and prospective therapeutic leads with structure-dependent anti-cancer actions and considerable promise in cell migration and proliferation suppression.

6.2.2 Targeting protein degradation as a strategy against cancer

Since the 2004 Nobel Prize in Chemistry was awarded for the discovery of ubiquitin-mediated protein degradation, novel strategies for protein degradation have been gradually investigated upon the above mechanism by pharmaceutical

researchers.

Interestingly, we found that NCA decreased the total protein level and surface of BST-2. Since previous data indicated that BST-2 is rapidly recycled at the cell surface[126], it is conceivable that NCA could prevent the recycling of endocytosed BST-2 back to the cell surface and the premise was that we found that NCA did not affect the transcription level of BST-2. Whether proteasomal or lysosomal pathways are involved in this process, we further used lysosomal inhibitors Bafilomycin A1 (BFA)[127] or Chloroquine (CQ)[128] and the NCA-mediated downregulation of BST-2 was significantly inhibited by the lysosomal inhibitor BFA or CQ, but not treatment with the proteasome inhibitor MG132, which confirmed that NCA promoted BST-2 degradation via lysosomal degradation pathway. These results were similar to the Vpn mediated BST-2 degradation reported by Janet L. Douglas et al[129]. They found that Vpu reduced cell surface and total steady-state BST-2 levels, treatment of cells with the lysosome acidification inhibitor concanamycin A, but not treatment with the proteasome inhibitor MG132, reduced BST-2 downregulation by wild-type Vpu, thereby suggesting that the presence of Vpu leads to the degradation of BST-2 via an endosome-lysosome degradation pathway. Most of studies showed the close correlation between BST-2 downregulation and the enhanced release of HIV-1, and silencing of BST-2 expression in HeLa cells by siRNA or shRNA rendered virus release from these cells Vpu-independent[68, 70], thus whether NCA could counter the tethering function of BST-2, resulting in enhanced HIV-1 virion release remains interesting to be investigated. Besides, from the immunostaining assay, we found that the distribution of BST-2 with NCA treatment changed from a large area around the perinucleus to concentrated small pieces although accompanied by diminished fluorescence intensity of BST-2, which seems consistent with the endosome or ER staining.

Given that targeted protein degradation technology has evolved a brand-new therapeutic modality from an innovative drug discovery perspective, and with this aim to develop novel strategy, proteolysis-targeting chimeras (PROTACs), which contains two linked moieties with one binding the protein of interest (POI) and the other binding

an E3 ligase, has become a promising new paradigm in chemical biology and drug development[130]. Nevertheless, to supplement the existing PROTACs, a variety of other strategies for targeted protein degradation have been investigated, such as lysosome-based strategies, which suggest a key direction for novel therapeutic approaches and unlock the magic toolbox for protein degradation technologies[131].

6.2.3 BST-2 as a novel druggable target

Extensive attempts have been taken to map cancer dependence by discovering genes that, when functionally inactivated, impede the development of cancer cells and are therefore potential treatment targets[132]. These studies have led to the identification of many protein-coding genes, which are potential cancer targets[132-134]. The Sanger Institute identified 627 priority targets, of which 232 are enzymes (37%)[134], and these have been the focus of developing small-molecule anticancer drugs.

BST-2 is overexpressed in different cancer cells and in recent decades, BST-2 attracted much attention for cancer research. Using genetic BST-2 KO and subsequent reconstitution, we identified that BST-2 played a key role in the anti-proliferative effect of NCA. Nonetheless, we found that knockdown of BST-2 in HeLa cell did not affect the cell proliferation and the KO clones, which we randomly selected for the further study, also showed little or no phenotypes in terms of cell proliferation. First, to exclude the clonal difference, we thawed more BST-2 KO clones and compared their cell proliferation capacity to that of WT cell line. As expected, in some clones, the BST-2 KO exhibited potent anti-proliferative properties against HeLa cells although the degree of inhibition was varying (Supplementary Figure 5). While this work was in preparation, other papers involving the effect of BST-2 on cell proliferation were published. As is consistent with our data, Wadie D Mahauad-Fernandez concluded that BST-2 suppression in murine cancer cells had no influence on cell proliferation in two-dimensional culture despite it reduced the capacity to grow independent of anchor[89]. In contrast, Shoichiro Mukai demonstrated that the growth of BST-2 small interfering RNA (siRNA)-transfected GC cells was

significantly slower than the growth of negative control siRNA-transfected GC cells[90]. Besides, Aejaz Sayeed et al. showed that exogenous overexpression of BST-2 promoted cell proliferation[135]. Yoshinori Shigematsu et al indicated that BST-2 small interfering RNA (siRNA)-transfected T24 cells exhibited significantly reduced cell growth relative to negative control siRNA-transfected T24 cells in MTT assays[136]. Based on the above distinction, we believed that this discrepancy may be due to cell type and different experimental systems. To exclude the effect of cell type in our system, we also detect the effect of BST-2 KD in liver cancer cell line HepG2. As expected, BST-2 KD significantly decreased the cell proliferation in HepG2 cells (Supplementary Figure 6), which fits our assumptions.

The epidermal growth factor receptor (EGFR), also known as ErbB1/HER1, is the prototype of the EGFR family that also includes ErbB2/HER2/Neu, ErbB3/HER3, and ErbB4/HER4[137] and is commonly upregulated in multiple cancers[138]. The aberrations of EGFR over-activate downstream pro-oncogenic signaling pathways, including the ERK MAPK, PI3K-AKTand JAK-STAT pathways and these pathways subsequently trigger a variety of biological outputs that promote cancer cell proliferation. To define the mechanism by which BST-2 activation promotes cancer cell proliferation, we have identified EGFRs as the key mediators and revealed that BST-2 KO diminished the phosphorylation of EGFR and its downstream signaling pathway the phosphorylation of STAT3, but not the phosphorylation of ERK. Coincidentally, one publication also reported that the levels of phosphorylated EGFR, ERK and Akt were lower in BST-2 siRNA-transfected GC cells than in control cells[90]. Yoshinori Shigematsu et al. also showed that the levels of phosphorylated Akt and ERK were lower in BST-2 siRNA-transfected T24 cells than in control cells[136]. However, regarding upregulation of the phosphorylation of ERK in BST-2 KO clones, we supposed that compensation pathways were activated due to BST-2 KO or downregulation. Beside this aspect, we also found a consistent regulation of the EGFR signaling pathway in the NCA-treated HeLa cells, which further confirmed BST-2 is likely to be the target of NCA.

6.2.4 Future Perspectives

6.2.4.1 Are modifications of BST-2 structure essential for NCA treatment?

BST-2 was proposed as a promising target of NCA in the ABPP experiment, and using knockdown or knockout and subsequent over-expression, we confirmed that NCA targeted BST-2 to exert potent anti-proliferative effect against cancer cells; however, we still do not know how NCA bound to BST-2 and affected its expression and function.

BST-2 forms stable cysteine-linked dimers[67], and is modified by N-linked glycosylation[65, 67], the N-terminus of the human BST-2 extracellular domain contains three cysteine residues at locations 53, 63, and 91 that control the assembly of covalently coupled BST-2 homodimers[139]. BST-2 dimers have been shown in previous studies to protect against viral infection and any one of three cysteine residues present in the BST-2 extracellular domain was sufficient for BST-2 dimerization. In contrast, BST-2 lacking all three cysteines in its ectodomain was unable to prevent release of HIV-1 virions[140]. Interestingly lack of dimerization did not prevent surface expression of BST-2. In addition, we also notice that the importance of BST-2 dimerization has been disputed[141]. Regarding the assessment of the involvement of BST-2 dimerization in altering cancer cell behavior, Wadie D Mahauad-Ternandez et al demonstrated that the roles of BST-2 involvement in promoting breast cancer appear to be connected to its structure, specifically covalent interactions between cysteine residues in the extracellular domain of BST-2 and they also revealed that BST-2 dimerization disruption prevented breast cancer cells from adhering to each other, immune cells, and ECM substrates[142]. Taken together, BST-2 dimerization plays a role in its antitumor effects.

For the glycosylation of BST-2, however, Amy J Andrew et al revealed that N-linked glycosylation was not crucial for inhibiting HIV-1 viral release, nor did it change surface expression or Vpu sensitivity. Given that BST-2/HM1.24 possesses two potential sites for N-glycosylation in the extra cytosolic domains of the proteins, from

our Western blot data with a BST-2-specific antibody, we always observed multiple immunoreactive bands in the range of 36–64 kDa consistent with the putative monomeric (36-kDa) and dimeric (64-kDa) glycosylated forms of BST-2 that have previously been described by others[66, 67]. Interestingly, we found that NCA decreased both the expression level of monomeric (36-kDa) and dimeric (64-kDa) glycosylated forms of BST-2. Up to date, the role of the glycosylation of BST-2 in cancer progression remains unclear.

6.2.4.2 Lipid rafts as potential target in cancer therapy

Last but not least, we found that NCA regulated EGFR protein dynamics and its downstream signaling via modulating lipid rafts function, although the mechanism remains elusive. In 1997, Simon and Ikonen[143] proposed the lipid rafts hypothesis, and they characterized lipid rafts as dynamic membrane microdomains enriched in glycosphingolipids and cholesterol and float freely within the fluid bilayer of cellular membranes, which expanded on Singer and Nicolson's fluid mosaic model of the cell membrane[144]. The Keystone Symposium on Lipid Rafts and Cell Function in 2006 presented the following definition of a lipid raft: lipid rafts are small (10-200 nm), heterogeneous, highly dynamic, sphingolipids and cholesterol-enriched lipid domains in the cell membrane that compartmentalize cellular processes[145]. Interestingly, it has been found that cancer cells exhibited higher amounts of membrane lipid rafts and cholesterol[146], including human prostate and breast cancer cell lines and they found that when compared with their non-tumorigenic cell line counterparts (PZ-HPV7 and MCF-10A), several human prostate and breast cancer cell lines (PC-3, LNCaP, MCF-7, and MDA-MB-231) exhibited increased cholesterol and GM1 staining, which was measured by filipin staining and binding of Alexa 568-conjugated choleratoxin-B subunit to detect plasma membrane cholesterol and lipid rafts, respectively[146]. Besides, it has also been shown that tumorigenic melanoma cells exhibit 1.5- to 2-fold greater cholesterol and raft levels than non-tumorigenic melanoma cells[147]. This

increase of the lipid rafts in cancer cells can be explained that lipid rafts serve as concentrating platforms for several signaling pathways and they harbor many cancer-related signaling and adhesion molecules[148].

Recently, more and more researchers have considered the potential of lipid rafts modulation as a promising target in cancer therapy. Among these studies, a common approach of disrupting lipid rafts and studying their function is to change cholesterol levels or destroy sphingolipids in the cell membrane. Statins, which are used to treat hypercholesterolaemia, are frequently used reagents in these investigations[148]. For example, Simvastatin, either alone or in combination with other chemotherapy drugs, has been proven in several clinical studies to dramatically improve treatment outcomes and reduce death in patients with certain forms of cancer[149, 150]. Knowledge of lipid rafts and raft assisted signaling pathways would inspire us to choose strategies for cancer prevention, cure, and treatment utilizing natural compounds, or other types of therapy.

6.2.4.3 Outlook

Our findings suggest that NCA targets BST-2 protein and subsequently disrupts lipid rafts dynamics and down-regulates the EGFR signaling pathway to exert an anti-proliferative impact on cancer cells. Although further mechanism beyond the interaction between NCA and BTS-2 still needs to be studied, BST-2 has shown its potentiality as an anti-tumor target. Despite the fact that host defense relies heavily on innate immunity, several innate immune genes perform contradictory roles in cancer prevention and/or promotion via unknown pathways. BST-2 is a unique innate immunity gene that has both antiviral and pro-tumor effects, thus it can serve as a model for studying the involvement of innate immunity genes in cancer.

REFERENCES

7. References

1. Bray F, Laversanne M, Weiderpass E, Soerjomataram I. The ever-increasing importance of cancer as a leading cause of premature death worldwide. Cancer. 2021;127: 3029-3030.
2. Sung H, Ferlay J, Siegel RL, et al. Global Cancer Statistics 2020: GLOBOCAN Estimates of Incidence and Mortality Worldwide for 36 Cancers in 185 Countries. CA Cancer J Clin. 2021;71: 209-249.
3. Omran AR. The epidemiologic transition. A theory of the epidemiology of population change. Milbank Mem Fund Q. 1971;49: 509-538.
4. Yabroff KR, Wu XC, Negoita S, et al. Association of the COVID-19 Pandemic With Patterns of Statewide Cancer Services. J Natl Cancer Inst. 2022;114: 907-909.
5. Hanahan D, Weinberg RA. Hallmarks of cancer: the next generation. Cell. 2011;144: 646-674.
6. Evan GI, Vousden KH. Proliferation, cell cycle and apoptosis in cancer. Nature. 2001;411: 342-348.
7. Hainaut P, Plymoth A. Targeting the hallmarks of cancer: towards a rational approach to next-generation cancer therapy. Curr Opin Oncol. 2013;25: 50-51.
8. Widmer N, Bardin C, Chatelut E, et al. Review of therapeutic drug monitoring of anticancer drugs part two--targeted therapies. Eur J Cancer. 2014;50: 2020-2036.
9. Vasan N, Baselga J, Hyman DM. A view on drug resistance in cancer. Nature. 2019;575: 299-309.
10. Newman DJ, Cragg GM. Natural Products as Sources of New Drugs over the Nearly Four Decades from 01/1981 to 09/2019. J Nat Prod. 2020;83: 770-803.
11. Huang MY, Zhang LL, Ding J, Lu JJ. Anticancer drug discovery from Chinese medicinal herbs. Chin Med. 2018;13: 35.
12. Yang CH, Horwitz SB. Taxol((R)): The First Microtubule Stabilizing Agent. Int J Mol Sci. 2017;18.
13. Chang J, Kim Y, Kwon HJ. Advances in identification and validation of protein targets of natural products without chemical modification. Nat Prod Rep. 2016;33: 719-730.
14. Charyulu EM, Sekaran G, Rajakumar GS, Gnanamani A. Antimicrobial activity of secondary metabolite from marine isolate, Pseudomonas sp. against Gram positive and negative bacteria including MRSA. Indian J Exp Biol. 2009;47: 964-968.
15. Cardellina JH, Moore BS. Richard E. Moore (1933-2007). J Nat Prod. 2010;73: 301-302.
16. Linington RG, Clark BR, Trimble EE, et al. Antimalarial peptides from marine cyanobacteria: isolation and structural elucidation of gallinamide A. J Nat Prod. 2009;72: 14-17.
17. Jaspars M, Lawton LA. Cyanobacteria - a novel source of pharmaceuticals. Curr Opin Drug Discov Devel. 1998;1: 77-84.
18. Tripathi A, Puddick J, Prinsep MR, Rottmann M, Tan LT. Lagunamides A and B: cytotoxic and antimalarial cyclodepsipeptides from the marine cyanobacterium Lyngbya majuscula. J Nat Prod. 2010;73: 1810-1814.
19. Sato S, Murata A, Orihara T, et al. Marine natural product aurilide activates the OPA1-mediated apoptosis by binding to prohibitin. Chem Biol. 2011;18: 131-139.
20. Han B, Gross H, Goeger DE, Mooberry SL, Gerwick WH. Aurilides B and C, cancer cell toxins from a Papua New Guinea collection of the marine cyanobacterium Lyngbya majuscula. J Nat Prod. 2006;69: 572-575.
21. Tripathi A, Fang W, Leong DT, Tan LT. Biochemical studies of the lagunamides, potent cytotoxic cyclic depsipeptides from the marine cyanobacterium Lyngbya majuscula. Mar Drugs. 2012;10: 1126-1137.
22. Michon S, Cavelier F, Salom-Roig XJ. Synthesis and Biological Activities of Cyclodepsipeptides of

Aurilide Family from Marine Origin. Mar Drugs. 2021;19.
23. Huang X, Huang W, Li L, et al. Structure Determinants of Lagunamide A for Anticancer Activity and Its Molecular Mechanism of Mitochondrial Apoptosis. Mol Pharm. 2016;13: 3756-3763.
24. Gleissner CM, Pyka CL, Heydenreuter W, et al. Neocarzilin A Is a Potent Inhibitor of Cancer Cell Motility Targeting VAT-1 Controlled Pathways. ACS Cent Sci. 2019;5: 1170-1178.
25. Xu PX, Adams J, Peters H, Brown MC, Heaney S, Maas R. Eya1-deficient mice lack ears and kidneys and show abnormal apoptosis of organ primordia. Nat Genet. 1999;23: 113-117.
26. Schonberger J, Wang L, Shin JT, et al. Mutation in the transcriptional coactivator EYA4 causes dilated cardiomyopathy and sensorineural hearing loss. Nat Genet. 2005;37: 418-422.
27. Grifone R, Demignon J, Giordani J, et al. Eya1 and Eya2 proteins are required for hypaxial somitic myogenesis in the mouse embryo. Dev Biol. 2007;302: 602-616.
28. El-Hashash AH, Al Alam D, Turcatel G, Bellusci S, Warburton D. Eyes absent 1 (Eya1) is a critical coordinator of epithelial, mesenchymal and vascular morphogenesis in the mammalian lung. Dev Biol. 2011;350: 112-126.
29. Wu K, Li Z, Cai S, et al. EYA1 phosphatase function is essential to drive breast cancer cell proliferation through cyclin D1. Cancer Res. 2013;73: 4488-4499.
30. Yuan B, Cheng L, Chiang HC, et al. A phosphotyrosine switch determines the antitumor activity of ERbeta. J Clin Invest. 2014;124: 3378-3390.
31. Pandey RN, Rani R, Yeo EJ, et al. The Eyes Absent phosphatase-transactivator proteins promote proliferation, transformation, migration, and invasion of tumor cells. Oncogene. 2010;29: 3715-3722.
32. Krueger AB, Drasin DJ, Lea WA, et al. Allosteric inhibitors of the Eya2 phosphatase are selective and inhibit Eya2-mediated cell migration. J Biol Chem. 2014;289: 16349-16361.
33. Wang Y, Pandey RN, Riffle S, Chintala H, Wikenheiser-Brokamp KA, Hegde RS. The Protein Tyrosine Phosphatase Activity of Eyes Absent Contributes to Tumor Angiogenesis and Tumor Growth. Mol Cancer Ther. 2018;17: 1659-1669.
34. Okabe Y, Sano T, Nagata S. Regulation of the innate immune response by threonine-phosphatase of Eyes absent. Nature. 2009;460: 520-524.
35. Liu X, Sano T, Guan Y, Nagata S, Hoffmann JA, Fukuyama H. Drosophila EYA regulates the immune response against DNA through an evolutionarily conserved threonine phosphatase motif. PLoS One. 2012;7: e42725.
36. Pignoni F, Hu B, Zavitz KH, Xiao J, Garrity PA, Zipursky SL. The eye-specification proteins So and Eya form a complex and regulate multiple steps in Drosophila eye development. Cell. 1997;91: 881-891.
37. Ohto H, Kamada S, Tago K, et al. Cooperation of six and eya in activation of their target genes through nuclear translocation of Eya. Mol Cell Biol. 1999;19: 6815-6824.
38. Heanue TA, Reshef R, Davis RJ, et al. Synergistic regulation of vertebrate muscle development by Dach2, Eya2, and Six1, homologs of genes required for Drosophila eye formation. Genes Dev. 1999;13: 3231-3243.
39. Silver SJ, Davies EL, Doyon L, Rebay I. Functional dissection of eyes absent reveals new modes of regulation within the retinal determination gene network. Mol Cell Biol. 2003;23: 5989-5999.
40. Xu PX, Cheng J, Epstein JA, Maas RL. Mouse Eya genes are expressed during limb tendon development and encode a transcriptional activation function. Proc Natl Acad Sci U S A. 1997;94: 11974-11979.
41. Coletta RD, Christensen K, Reichenberger KJ, et al. The Six1 homeoprotein stimulates tumorigenesis by reactivation of cyclin A1. Proc Natl Acad Sci U S A. 2004;101: 6478-6483.

42. Li Z, Tian T, Lv F, et al. Six1 promotes proliferation of pancreatic cancer cells via upregulation of cyclin D1 expression. PLoS One. 2013;8: e59203.
43. Wang CA, Jedlicka P, Patrick AN, et al. SIX1 induces lymphangiogenesis and metastasis via upregulation of VEGF-C in mouse models of breast cancer. J Clin Invest. 2012;122: 1895-1906.
44. Micalizzi DS, Christensen KL, Jedlicka P, et al. The Six1 homeoprotein induces human mammary carcinoma cells to undergo epithelial-mesenchymal transition and metastasis in mice through increasing TGF-beta signaling. J Clin Invest. 2009;119: 2678-2690.
45. Tootle TL, Silver SJ, Davies EL, et al. The transcription factor Eyes absent is a protein tyrosine phosphatase. Nature. 2003;426: 299-302.
46. Shimasaki N, Watanabe K, Hara M, Kosaki K. EYA1 mutation in a newborn female presenting with cardiofacial syndrome. Pediatr Cardiol. 2004;25: 411-413.
47. Azuma N, Hirakiyama A, Inoue T, Asaka A, Yamada M. Mutations of a human homologue of the Drosophila eyes absent gene (EYA1) detected in patients with congenital cataracts and ocular anterior segment anomalies. Hum Mol Genet. 2000;9: 363-366.
48. Robin TP, Smith A, McKinsey E, Reaves L, Jedlicka P, Ford HL. EWS/FLI1 regulates EYA3 in Ewing sarcoma via modulation of miRNA-708, resulting in increased cell survival and chemoresistance. Mol Cancer Res. 2012;10: 1098-1108.
49. Kim YH, Lee HC, Kim SY, et al. Epigenomic analysis of aberrantly methylated genes in colorectal cancer identifies genes commonly affected by epigenetic alterations. Ann Surg Oncol. 2011;18: 2338-2347.
50. Zhang L, Yang N, Huang J, et al. Transcriptional coactivator Drosophila eyes absent homologue 2 is up-regulated in epithelial ovarian cancer and promotes tumor growth. Cancer Res. 2005;65: 925-932.
51. Miller SJ, Lan ZD, Hardiman A, et al. Inhibition of Eyes Absent Homolog 4 expression induces malignant peripheral nerve sheath tumor necrosis. Oncogene. 2010;29: 368-379.
52. Li CM, Guo M, Borczuk A, et al. Gene expression in Wilms' tumor mimics the earliest committed stage in the metanephric mesenchymal-epithelial transition. Am J Pathol. 2002;160: 2181-2190.
53. Zhang L, Zhou H, Li X, et al. Eya3 partners with PP2A to induce c-Myc stabilization and tumor progression. Nat Commun. 2018;9: 1047.
54. Wang Y, Pandey RN, Roychoudhury K, et al. Targeting EYA3 in Ewing Sarcoma Retards Tumor Growth and Angiogenesis. Mol Cancer Ther. 2021;20: 803-815.
55. Farabaugh SM, Micalizzi DS, Jedlicka P, Zhao R, Ford HL. Eya2 is required to mediate the pro-metastatic functions of Six1 via the induction of TGF-beta signaling, epithelial-mesenchymal transition, and cancer stem cell properties. Oncogene. 2012;31: 552-562.
56. Tadjuidje E, Wang TS, Pandey RN, Sumanas S, Lang RA, Hegde RS. The EYA tyrosine phosphatase activity is pro-angiogenic and is inhibited by benzbromarone. PLoS One. 2012;7: e34806.
57. Krishnan N, Jeong DG, Jung SK, et al. Dephosphorylation of the C-terminal tyrosyl residue of the DNA damage-related histone H2A.X is mediated by the protein phosphatase eyes absent. J Biol Chem. 2009;284: 16066-16070.
58. Mentel M, Ionescu AE, Puscalau-Girtu I, et al. WDR1 is a novel EYA3 substrate and its dephosphorylation induces modifications of the cellular actin cytoskeleton. Sci Rep. 2018;8: 2910.
59. Xiao A, Li H, Shechter D, et al. WSTF regulates the H2A.X DNA damage response via a novel tyrosine kinase activity. Nature. 2009;457: 57-62.
60. Cook PJ, Ju BG, Telese F, Wang X, Glass CK, Rosenfeld MG. Tyrosine dephosphorylation of H2AX modulates apoptosis and survival decisions. Nature. 2009;458: 591-596.

61. Ishikawa J, Kaisho T, Tomizawa H, et al. Molecular cloning and chromosomal mapping of a bone marrow stromal cell surface gene, BST2, that may be involved in pre-B-cell growth. Genomics. 1995;26: 527-534.
62. Habermann A, Krijnse-Locker J, Oberwinkler H, et al. CD317/tetherin is enriched in the HIV-1 envelope and downregulated from the plasma membrane upon virus infection. J Virol. 2010;84: 4646-4658.
63. Sauter D. Counteraction of the multifunctional restriction factor tetherin. Front Microbiol. 2014;5: 163.
64. Cole G, Simonetti K, Ademi I, Sharpe S. Dimerization of the transmembrane domain of human tetherin in membrane mimetic environments. Biochemistry. 2012;51: 5033-5040.
65. Kupzig S, Korolchuk V, Rollason R, Sugden A, Wilde A, Banting G. Bst-2/HM1.24 is a raft-associated apical membrane protein with an unusual topology. Traffic. 2003;4: 694-709.
66. Goto T, Kennel SJ, Abe M, et al. A novel membrane antigen selectively expressed on terminally differentiated human B cells. Blood. 1994;84: 1922-1930.
67. Ohtomo T, Sugamata Y, Ozaki Y, et al. Molecular cloning and characterization of a surface antigen preferentially overexpressed on multiple myeloma cells. Biochem Biophys Res Commun. 1999;258: 583-591.
68. Neil SJ, Zang T, Bieniasz PD. Tetherin inhibits retrovirus release and is antagonized by HIV-1 Vpu. Nature. 2008;451: 425-430.
69. Jones PH, Mehta HV, Maric M, Roller RJ, Okeoma CM. Bone marrow stromal cell antigen 2 (BST-2) restricts mouse mammary tumor virus (MMTV) replication in vivo. Retrovirology. 2012;9: 10.
70. Van Damme N, Goff D, Katsura C, et al. The interferon-induced protein BST-2 restricts HIV-1 release and is downregulated from the cell surface by the viral Vpu protein. Cell Host Microbe. 2008;3: 245-252.
71. Klimkait T, Strebel K, Hoggan MD, Martin MA, Orenstein JM. The human immunodeficiency virus type 1-specific protein vpu is required for efficient virus maturation and release. J Virol. 1990;64: 621-629.
72. Varthakavi V, Smith RM, Bour SP, Strebel K, Spearman P. Viral protein U counteracts a human host cell restriction that inhibits HIV-1 particle production. Proc Natl Acad Sci U S A. 2003;100: 15154-15159.
73. Miyagi E, Andrew AJ, Kao S, Strebel K. Vpu enhances HIV-1 virus release in the absence of Bst-2 cell surface down-modulation and intracellular depletion. Proc Natl Acad Sci U S A. 2009;106: 2868-2873.
74. Douglas JL, Gustin JK, Viswanathan K, Mansouri M, Moses AV, Fruh K. The great escape: viral strategies to counter BST-2/tetherin. PLoS Pathog. 2010;6: e1000913.
75. Galao RP, Le Tortorec A, Pickering S, Kueck T, Neil SJ. Innate sensing of HIV-1 assembly by Tetherin induces NFkappaB-dependent proinflammatory responses. Cell Host Microbe. 2012;12: 633-644.
76. Tokarev A, Suarez M, Kwan W, Fitzpatrick K, Singh R, Guatelli J. Stimulation of NF-kappaB activity by the HIV restriction factor BST2. J Virol. 2013;87: 2046-2057.
77. Li SX, Barrett BS, Heilman KJ, et al. Tetherin promotes the innate and adaptive cell-mediated immune response against retrovirus infection in vivo. J Immunol. 2014;193: 306-316.
78. Walter-Yohrling J, Cao X, Callahan M, et al. Identification of genes expressed in malignant cells that promote invasion. Cancer Res. 2003;63: 8939-8947.
79. Cai D, Cao J, Li Z, et al. Up-regulation of bone marrow stromal protein 2 (BST2) in breast cancer with bone metastasis. BMC Cancer. 2009;9: 102.

80. Yokoyama T, Enomoto T, Serada S, et al. Plasma membrane proteomics identifies bone marrow stromal antigen 2 as a potential therapeutic target in endometrial cancer. Int J Cancer. 2013;132: 472-484.
81. Wang W, Nishioka Y, Ozaki S, et al. HM1.24 (CD317) is a novel target against lung cancer for immunotherapy using anti-HM1.24 antibody. Cancer Immunol Immunother. 2009;58: 967-976.
82. Fang KH, Kao HK, Chi LM, et al. Overexpression of BST2 is associated with nodal metastasis and poorer prognosis in oral cavity cancer. Laryngoscope. 2014;124: E354-360.
83. Wainwright DA, Balyasnikova IV, Han Y, Lesniak MS. The expression of BST2 in human and experimental mouse brain tumors. Exp Mol Pathol. 2011;91: 440-446.
84. Schliemann C, Roesli C, Kamada H, et al. In vivo biotinylation of the vasculature in B-cell lymphoma identifies BST-2 as a target for antibody-based therapy. Blood. 2010;115: 736-744.
85. Ozaki S, Kosaka M, Wakahara Y, et al. Humanized anti-HM1.24 antibody mediates myeloma cell cytotoxicity that is enhanced by cytokine stimulation of effector cells. Blood. 1999;93: 3922-3930.
86. Ono K, Ohtomo T, Yoshida K, et al. The humanized anti-HM1.24 antibody effectively kills multiple myeloma cells by human effector cell-mediated cytotoxicity. Mol Immunol. 1999;36: 387-395.
87. Tai YT, Horton HM, Kong SY, et al. Potent in vitro and in vivo activity of an Fc-engineered humanized anti-HM1.24 antibody against multiple myeloma via augmented effector function. Blood. 2012;119: 2074-2082.
88. Ozaki S, Kosaka M, Wakatsuki S, Abe M, Koishihara Y, Matsumoto T. Immunotherapy of multiple myeloma with a monoclonal antibody directed against a plasma cell-specific antigen, HM1.24. Blood. 1997;90: 3179-3186.
89. Mahauad-Fernandez WD, DeMali KA, Olivier AK, Okeoma CM. Bone marrow stromal antigen 2 expressed in cancer cells promotes mammary tumor growth and metastasis. Breast Cancer Res. 2014;16: 493.
90. Mukai S, Oue N, Oshima T, et al. Overexpression of Transmembrane Protein BST2 is Associated with Poor Survival of Patients with Esophageal, Gastric, or Colorectal Cancer. Ann Surg Oncol. 2017;24: 594-602.
91. Yi EH, Yoo H, Noh KH, et al. BST-2 is a potential activator of invasion and migration in tamoxifen-resistant breast cancer cells. Biochem Biophys Res Commun. 2013;435: 685-690.
92. Billcliff PG, Rollason R, Prior I, Owen DM, Gaus K, Banting G. CD317/tetherin is an organiser of membrane microdomains. J Cell Sci. 2013;126: 1553-1564.
93. Lingwood D, Simons K. Lipid rafts as a membrane-organizing principle. Science. 2010;327: 46-50.
94. Yarden Y, Sliwkowski MX. Untangling the ErbB signalling network. Nat Rev Mol Cell Biol. 2001;2: 127-137.
95. Wang Z. ErbB Receptors and Cancer. Methods Mol Biol. 2017;1652: 3-35.
96. Chong CR, Janne PA. The quest to overcome resistance to EGFR-targeted therapies in cancer. Nat Med. 2013;19: 1389-1400.
97. Mineo C, James GL, Smart EJ, Anderson RG. Localization of epidermal growth factor-stimulated Ras/Raf-1 interaction to caveolae membrane. J Biol Chem. 1996;271: 11930-11935.
98. Mineo C, Gill GN, Anderson RG. Regulated migration of epidermal growth factor receptor from caveolae. J Biol Chem. 1999;274: 30636-30643.
99. Lambert S, Ameels H, Gniadecki R, Herin M, Poumay Y. Internalization of EGF receptor following lipid rafts disruption in keratinocytes is delayed and dependent on p38 MAPK activation. J Cell Physiol. 2008;217: 834-845.

100. Castillo J, Erroba E, Perugorria MJ, et al. Amphiregulin contributes to the transformed phenotype of human hepatocellular carcinoma cells. Cancer Res. 2006;66: 6129-6138.
101. Zhang G, Li X, Chen Q, et al. CD317 Activates EGFR by Regulating Its Association with Lipid Rafts. Cancer Res. 2019;79: 2220-2231.
102. Ran FA, Hsu PD, Wright J, Agarwala V, Scott DA, Zhang F. Genome engineering using the CRISPR-Cas9 system. Nat Protoc. 2013;8: 2281-2308.
103. Riccardi C, Nicoletti I. Analysis of apoptosis by propidium iodide staining and flow cytometry. Nat Protoc. 2006;1: 1458-1461.
104. McBride HM, Neuspiel M, Wasiak S. Mitochondria: more than just a powerhouse. Curr Biol. 2006;16: R551-560.
105. Gorges J, Kazmaier U. Matteson Homologation-Based Total Synthesis of Lagunamide A. Org Lett. 2018;20: 2033-2036.
106. Tewey KM, Rowe TC, Yang L, Halligan BD, Liu LF. Adriamycin-induced DNA damage mediated by mammalian DNA topoisomerase II. Science. 1984;226: 466-468.
107. Mah LJ, El-Osta A, Karagiannis TC. gammaH2AX: a sensitive molecular marker of DNA damage and repair. Leukemia. 2010;24: 679-686.
108. Roos WP, Thomas AD, Kaina B. DNA damage and the balance between survival and death in cancer biology. Nat Rev Cancer. 2016;16: 20-33.
109. Zhao L, Zhao J, Zhong K, Tong A, Jia D. Targeted protein degradation: mechanisms, strategies and application. Signal Transduct Target Ther. 2022;7: 113.
110. Presle A, Fremont S, Salles A, et al. The viral restriction factor tetherin/BST2 tethers cytokinetic midbody remnants to the cell surface. Curr Biol. 2021;31: 2203-2213 e2205.
111. Cragg GM, Grothaus PG, Newman DJ. Impact of natural products on developing new anti-cancer agents. Chem Rev. 2009;109: 3012-3043.
112. Carnero Corrales MA, Zinken S, Konstantinidis G, et al. Thermal proteome profiling identifies the membrane-bound purinergic receptor P2X4 as a target of the autophagy inhibitor indophagolin. Cell Chem Biol. 2021;28: 1750-1757 e1755.
113. Kirsch VC, Orgler C, Braig S, et al. The Cytotoxic Natural Product Vioprolide A Targets Nucleolar Protein 14, Which Is Essential for Ribosome Biogenesis. Angew Chem Int Ed Engl. 2020;59: 1595-1600.
114. Koczian F, Naglo O, Vomacka J, et al. Targeting the endoplasmic reticulum-mitochondria interface sensitizes leukemia cells to cytostatics. Haematologica. 2019;104: 546-555.
115. Le P, Nodwell MB, Eirich J, Sieber SA. A Chemical Proteomic Analysis of Illudin-Interacting Proteins. Chemistry. 2019;25: 12644-12651.
116. Reinhardt T, Lee KM, Niederegger L, Hess CR, Sieber SA. Indolin-2-one Nitroimidazole Antibiotics Exhibit an Unexpected Dual Mode of Action. ACS Chem Biol. 2022;17: 3077-3085.
117. Cheeseman IM, Desai A. Molecular architecture of the kinetochore-microtubule interface. Nat Rev Mol Cell Biol. 2008;9: 33-46.
118. Yi F, Zhang Y, Wang Z, et al. The deacetylation-phosphorylation regulation of SIRT2-SMC1A axis as a mechanism of antimitotic catastrophe in early tumorigenesis. Sci Adv. 2021;7.
119. Shrivastav M, De Haro LP, Nickoloff JA. Regulation of DNA double-strand break repair pathway choice. Cell Res. 2008;18: 134-147.
120. Hanahan D. Hallmarks of Cancer: New Dimensions. Cancer Discov. 2022;12: 31-46.
121. Rayapureddi JP, Kattamuri C, Steinmetz BD, et al. Eyes absent represents a class of protein tyrosine phosphatases. Nature. 2003;426: 295-298.

122. Li X, Oghi KA, Zhang J, et al. Eya protein phosphatase activity regulates Six1-Dach-Eya transcriptional effects in mammalian organogenesis. Nature. 2003;426: 247-254.
123. Li Z, Qiu R, Qiu X, Tian T. EYA2 promotes lung cancer cell proliferation by downregulating the expression of PTEN. Oncotarget. 2017;8: 110837-110848.
124. Middleton MR, Margison GP. Improvement of chemotherapy efficacy by inactivation of a DNA-repair pathway. Lancet Oncol. 2003;4: 37-44.
125. Zamble DB, Lippard SJ. Cisplatin and DNA repair in cancer chemotherapy. Trends Biochem Sci. 1995;20: 435-439.
126. Rollason R, Korolchuk V, Hamilton C, Schu P, Banting G. Clathrin-mediated endocytosis of a lipid-raft-associated protein is mediated through a dual tyrosine motif. J Cell Sci. 2007;120: 3850-3858.
127. Mauvezin C, Neufeld TP. Bafilomycin A1 disrupts autophagic flux by inhibiting both V-ATPase-dependent acidification and Ca-P60A/SERCA-dependent autophagosome-lysosome fusion. Autophagy. 2015;11: 1437-1438.
128. Mauthe M, Orhon I, Rocchi C, et al. Chloroquine inhibits autophagic flux by decreasing autophagosome-lysosome fusion. Autophagy. 2018;14: 1435-1455.
129. Douglas JL, Viswanathan K, McCarroll MN, Gustin JK, Fruh K, Moses AV. Vpu directs the degradation of the human immunodeficiency virus restriction factor BST-2/Tetherin via a betaTrCP-dependent mechanism. J Virol. 2009;83: 7931-7947.
130. Zou Y, Ma D, Wang Y. The PROTAC technology in drug development. Cell Biochem Funct. 2019;37: 21-30.
131. Banik SM, Pedram K, Wisnovsky S, Ahn G, Riley NM, Bertozzi CR. Lysosome-targeting chimaeras for degradation of extracellular proteins. Nature. 2020;584: 291-297.
132. Tsherniak A, Vazquez F, Montgomery PG, et al. Defining a Cancer Dependency Map. Cell. 2017;170: 564-576 e516.
133. Hart T, Chandrashekhar M, Aregger M, et al. High-Resolution CRISPR Screens Reveal Fitness Genes and Genotype-Specific Cancer Liabilities. Cell. 2015;163: 1515-1526.
134. Behan FM, Iorio F, Picco G, et al. Prioritization of cancer therapeutic targets using CRISPR-Cas9 screens. Nature. 2019;568: 511-516.
135. Sayeed A, Luciani-Torres G, Meng Z, Bennington JL, Moore DH, Dairkee SH. Aberrant regulation of the BST2 (Tetherin) promoter enhances cell proliferation and apoptosis evasion in high grade breast cancer cells. PLoS One. 2013;8: e67191.
136. Shigematsu Y, Oue N, Nishioka Y, et al. Overexpression of the transmembrane protein BST-2 induces Akt and Erk phosphorylation in bladder cancer. Oncol Lett. 2017;14: 999-1004.
137. Pines G, Kostler WJ, Yarden Y. Oncogenic mutant forms of EGFR: lessons in signal transduction and targets for cancer therapy. FEBS Lett. 2010;584: 2699-2706.
138. Yarden Y, Pines G. The ERBB network: at last, cancer therapy meets systems biology. Nat Rev Cancer. 2012;12: 553-563.
139. Welbourn S, Kao S, Du Pont KE, Andrew AJ, Berndsen CE, Strebel K. Positioning of cysteine residues within the N-terminal portion of the BST-2/tetherin ectodomain is important for functional dimerization of BST-2. J Biol Chem. 2015;290: 3740-3751.
140. Andrew AJ, Miyagi E, Kao S, Strebel K. The formation of cysteine-linked dimers of BST-2/tetherin is important for inhibition of HIV-1 virus release but not for sensitivity to Vpu. Retrovirology. 2009;6: 80.
141. Sakuma T, Sakurai A, Yasuda J. Dimerization of tetherin is not essential for its antiviral activity

against Lassa and Marburg viruses. PLoS One. 2009;4: e6934.
142. Mahauad-Fernandez WD, Okeoma CM. Cysteine-linked dimerization of BST-2 confers anoikis resistance to breast cancer cells by negating proapoptotic activities to promote tumor cell survival and growth. Cell Death Dis. 2017;8: e2687.
143. Simons K, Ikonen E. Functional rafts in cell membranes. Nature. 1997;387: 569-572.
144. Singer SJ, Nicolson GL. The fluid mosaic model of the structure of cell membranes. Science. 1972;175: 720-731.
145. Pike LJ. Rafts defined: a report on the Keystone Symposium on Lipid Rafts and Cell Function. J Lipid Res. 2006;47: 1597-1598.
146. Li YC, Park MJ, Ye SK, Kim CW, Kim YN. Elevated levels of cholesterol-rich lipid rafts in cancer cells are correlated with apoptosis sensitivity induced by cholesterol-depleting agents. Am J Pathol. 2006;168: 1107-1118; quiz 1404-1105.
147. Levin-Gromiko U, Koshelev V, Kushnir P, Fedida-Metula S, Voronov E, Fishman D. Amplified lipid rafts of malignant cells constitute a target for inhibition of aberrantly active NFAT and melanoma tumor growth by the aminobisphosphonate zoledronic acid. Carcinogenesis. 2014;35: 2555-2566.
148. Simons K, Toomre D. Lipid rafts and signal transduction. Nat Rev Mol Cell Biol. 2000;1: 31-39.
149. Boudreau DM, Yu O, Johnson J. Statin use and cancer risk: a comprehensive review. Expert Opin Drug Saf. 2010;9: 603-621.
150. Di Bello E, Zwergel C, Mai A, Valente S. The Innovative Potential of Statins in Cancer: New Targets for New Therapies. Front Chem. 2020;8: 516.

APPENDIX

8. Appendix

8.1 Supplementary Material

8.1.1 Supplementary Figures

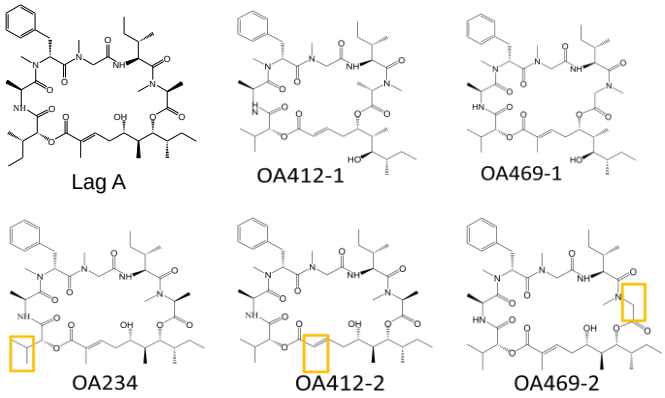

	Lag A	OA412-1	OA469-1	OA234	OA412-2	OA469-2
IC_{50} (nM)	7.898	≈100	＞100	10.25	8.643	36.09
EC_{50} (nM)	5.561	＞300	＞100	20.29	15.51	32.40

Supplementary Figure 1: Structure-activity relationship---Anti-proliferative and pro-apoptotic effects of Lag A and its analogues in Jurkat cells. (A) Chemical structure of Lag A and its analogues and the different part of the analogues from Lag A are marked in orange. (B) Proliferative capacity and pro-apoptotic effect of human cervix cancer HeLa cells treated with Lag A, OA412-1, OA469-1, OA234, OA412-2 and OA469-2. IC_{50} values were determined by crystal violet staining after 72 h and EC_{50} values were evaluated with Nicoletti assay after 48 h.

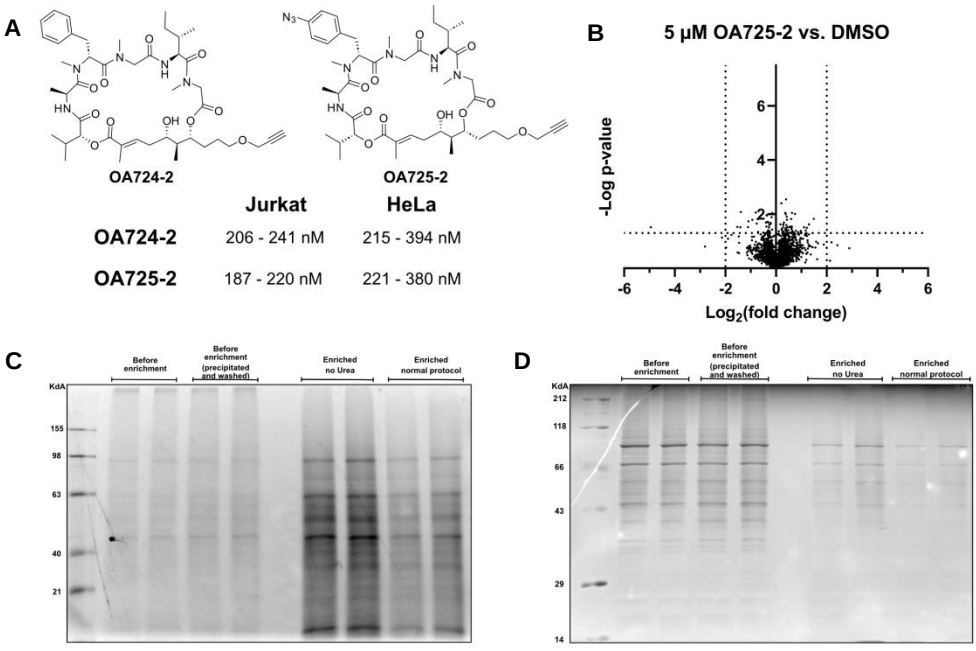

Supplementary Figure 2. Affinity based protein profiling using Lag A photo-affinity probes did not identify any protein targets. (A) Structure of the photo-affinity probe OA725-2 and its non-photo-affinity derivative OA724-2. IC_{50} of relative metabolic activity measured using MTT assay are given for HeLa and Jurkat cells (95 % CV). (B) Volcano-plot of HeLa lysate treated with 5 µM OA725-2 vs. DMSO. Dotted lines indicate cut-off at $p < 0.05$ and a Log_2 (fold change) > 2. (C) Fluorescent imaging of SDS-PAGE gel to visualise labelled proteins. HeLa lysate was treated with 5 µM OA725-2 for 30 min, UV irradiated and clicked to a trifunctional linker bearing a biotin and rhodamine moiety. Samples were taken before and after enrichment. Experiment was conducted in duplicates and using different enrichment protocols. (D) Coomassie stained SDS-PAGE gel. The same gel as in (C) but stained with Coomassie to visualise all proteins. Experiments were performed by Dietrich Mostert (Group of Prof. Sieber, Department of Chemistry, Technical University of Munich, Germany).

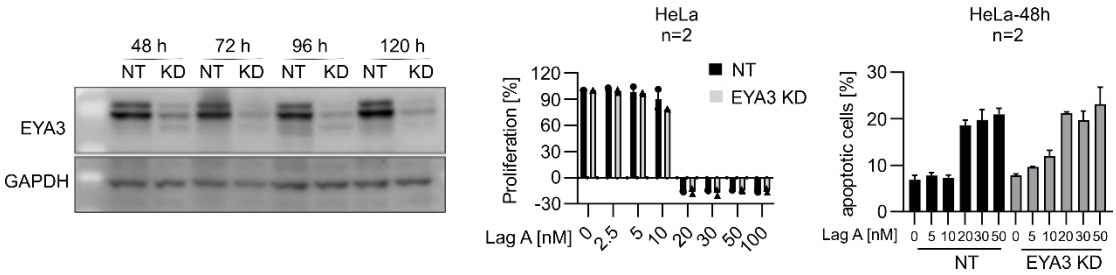

Supplementary Figure 3. EYA3 KD does not affect the anti-proliferative and pro-apoptotic effect of Lag A. (A) Western blot of EYA3 protein levels in non-targeting (NT) and EYA3 siRNA HeLa (KD) after 48, 72, 96 and 120 h transfection. (B) Anti-proliferative effect of Lag A in NT and EYA3 siRNA transfected HeLa (KD) cells was measured by crystal violet staining assay. Cells were treated with indicated concentrations of Lag A for 72 h. (C) Pro-apoptotic effect of Lag A in NT and EYA3 siRNA transfected (KD) HeLa cells was measured by Nicoletti assay. Cells were treated with indicated concentrations of Lag A for 48 h.

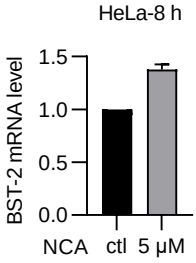

Supplementary Figure 4. NCA does not decrease BST-2 mRNA level. HeLa cells were treated with NCA or DMSO for 8 h and then mRNA was isolated for the downstream qPCR detection to measure the effect of NCA treatment on BST-2 mRNA level.

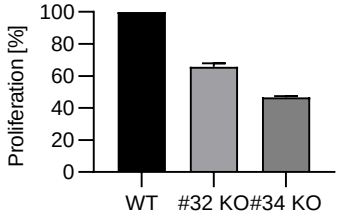

Supplementary Figure 5. BST-2 KO affects the cell proliferative in HeLa cells. Cell proliferation of WT and BST-2 KO (#32 and #34) cells was determined by crystal violet staining assay after 72 h.

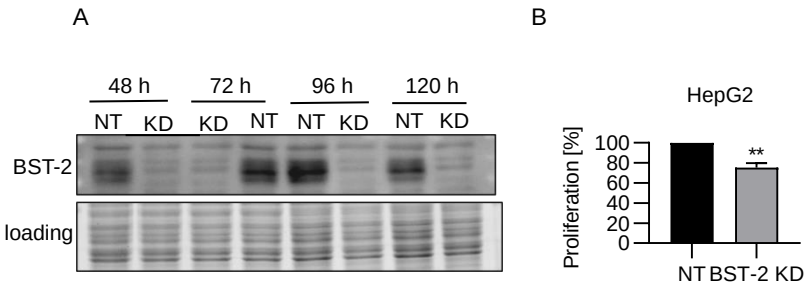

Supplementary Figure 6. BST-2 KD decreases the proliferation of HepG2. (A) Western blot of BST-2 protein levels in non-targeting (NT) and BST-2 siRNA HepG2 (KD) after 48, 72, 96 and 120 h transfection. (B) Cell proliferation of NT and BST-2 siRNA transfected HepG2 (KD) cells was determined by crystal violet staining assay after 72 h. Data are presented as means ± SEM, n=3, unpaired t-test with Welch's correction, **P<0.01.

8.1.2 Supplementary Scheme

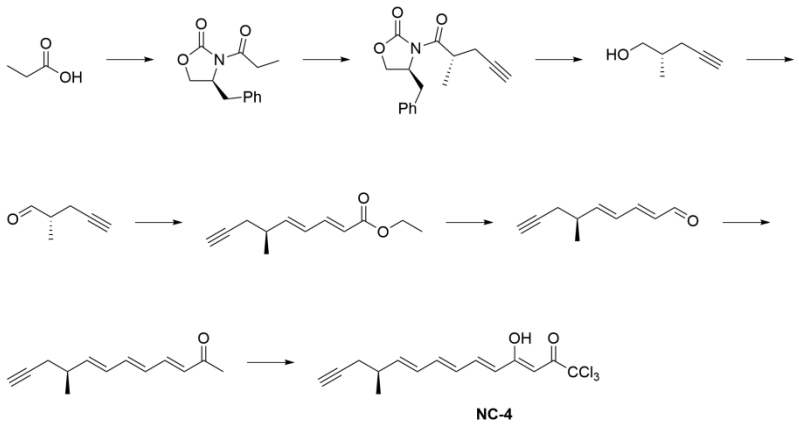

Supplementary Scheme 1. Synthesis procedure of NCA probe **NC-4**.

8.1.3 Supplementary Tables

Supplementary Table 1. Bliss synergy score

Bliss values (＞0 represents synergism)	DXR 1 μM	Synergistic effect
5 nM Lag A	12.23	Yes
10 nM Lag A	10.97	Yes

Supplementary Table 2. Listed proteins were significantly enriched in NC-4 treated cells in comparison to DMSO control treated cells. Experiment was performed by Josef Braun (Group of Prof. Sieber, Department of Chemistry, Technical University of Munich, Germany).

Sequence coverage [%]	-Log_{10} Student's T-test p-value	Gene	Protein
46.8	5.43993	HMOX2	Heme oxygenase 2

45.2	4.74889	CYB5B	Cytochrome b5 type B
2.4	4.46663	RTN1	Reticulon-1
48.9	3.84882	VAT1	Synaptic vesicle membrane protein VAT-1 homolog
9.5	3.33515	C16orf58	RUS1 family protein C16orf58
18.3	3.31682	BST-2	Bone marrow stromal antigen 2
13.2	3.12132	C18orf32	UPF0729 protein C18orf32
5.5	2.95102	SLC1A1	Amino acid transporter; Excitatory amino acid transporter 3
14.2	2.55273	ENDOD1	Endonuclease domain-containing 1 protein
15.2	2.08491	PIR	Pirin
15.1	1.99168	MCAM	Cell surface glycoprotein MUC18
20.8	1.81496	PRAF2	PRA1 family protein 2
21.9	1.59121	COTL1	Coactosin-like protein
6.6	1.55117	GAPVD1	GTPase-activating protein and VPS9 domain-containing protein 1
5.6	1.46378	PTGES	Prostaglandin E synthase
13.5	1.32317	CD63	Tetraspanin; CD63 antigen
20.9	1.30221	CD44	CD44 antigen

8.2 Abbreviations

ABPP	Activity-based protein profiling
ANOVA	Analysis of variance
APS	Ammonium persulfate
ATP	Adenosine triphosphate
Bcl-2	B-cell lymphoma 2
Bcl-xL	B-cell lymphoma extra large
BFA	Bafilomycin A1
BSA	Bovine serum albumin
CQ	Chloroquine
CRISPR	Clustered regularly interspaced short palindromic repeats
CTB	Cell titer blue
Ctl	Control
DMEM	Dulbecco's modified Eagle's Medium
DMSO	Dimethylsulfoxide
DNA	Desoxyribonucleic acid
DTT	Dithiothreitol
DXR	Doxorubicin
E.coli	Escherichia coli
EC50	Half-maximal effective concentration
ECL	Enhanced chemiluminescence
EDTA	Ethylenediaminetetraacetic acid
EGFR	Epidermal growth factor receptor

Em	Emission
ERK	Extracellular-signal regulated kinase
Ex	Excitation
FACS	Fluorescence activated cell sorting
FCCP	Carbonyl cyanide-4-(trifluoromethoxy)phenylhydrazone
FCS	Fetal calf serum
HRP	Horseradish peroxidase
IC50	Half-maximal inhibitory concentration
JC-1	Tetraethylbenzimidazolylcarbocyanine iodide
Lag A	Lagunamide A
LC-MS	Liquid chromatography–mass spectrometry
Mcl-1	Induced myeloid leukemia cell differentiation protein
Mfn1	Mitofusin 1
MMP	Mitochondrial membrane potential
NCA	Neocarzilin A
NP-40	Octoxinol 9
OCR	Oxygen consumption rate
OPA1	Optic atrophy 1
P/S	Penicillin/ streptomycin
PAA	Polyacrylamide
PAGE	Polyacrylamide gel electrophoresis
PBS	Phosphate-buffered saline
PCR	Polymerase chain reaction
PFA	Paraformaldehyde
PI	Propidium iodide
PVDF	Polyvinylidene difluoride
ROS	Reactive oxygen species
RPMI	Roswell Park Memorial Institute
RT	Room temperature
SAR	Structure-activity relationships study
SDS	Sodium dodecyl sulfate
siRNA	Small interfering RNA
STAT3	Signal transducer and activator of transcription 3
TBS-T	Tris-buffered saline + Tween
TCE	Trichloroethanol
TEM	Transmission electron microscopy
TPP	Thermal proteome profiling
WT	Wild type

8.3 List of publications and conference contributions

8.3.1 Article

Identification of EYA3 as a novel target for the natural compound Lagunamide A

Yudong Hu[1§], Dietrich Mostert[2§], Christina Orgler[1], Oliver Andler[3], Hans Zischka[4], Uli Kazmaier[3], Angelika M. Vollmar[1], Simone Braig[1], Stephan A. Sieber[2*], Stefan Zahler[1*]

Submitted

BST-2 is a novel target of the natural compound Neocarzilin A

Yudong Hu[1§], Josef Braun[2§], Angelika M. Vollmar, Stephan A. Sieber*, Stefan Zahler*

In preparation

8.3.2 Posters

19th World Congress of Basic & Clinical Pharmacology (WCP2023), July 2-7th, 2023, Glasgow, SCOTLAND

BST-2 is a novel target of the natural compound Neocarzilin A

Yudong Hu[1§], Josef Braun[2§], Angelika M. Vollmar, Stephan A. Sieber*, Stefan Zahler*

8.4 Acknowledgements

The sky is getting late, but the afterglow is still there. In this atmosphere, I draw the last period of this article. I look out of the window at the green leaves, the sun is shining brightly, and the wind is breezy, just like my mood---peace and joy. Time flies to four years ago when I first stepped into this land where I started my four-year Ph.D. study and life. Compared with that time, I am now much calmer and more confident in myself and the future. This confidence comes from the pursuit and expectation of a happy life all the time, from the exploration and accumulation of four years of doctoral life and study, and from the warmth and help I felt during this period of life. What virtues or abilities have I, everyone I meet is impartial and they can transmit wisdom, impart Knowledge and solve Doubts, besides, they are good teachers and helpful friends for me.

First of all, I should be most grateful to Professor Vollmar, thank you for replying to my email when I was far away in China, and for giving me the permission to embark on a doctoral career. If it weren't for your encouragement when my project was not lucky, I wouldn't be able to successfully complete my doctoral study now; I look forward to your guidance and help every time I report, and I can always gain a lot from you.

Secondly, I am very grateful to my project and thesis advisor Professor Zahler, who has condensed his hard work and wisdom from project research and experimental design to result analysis and article writing and thesis revision. Without his guidance and help to me, it would be difficult for me to overcome the ups and downs on the road of my academic research. A harmonious teacher-student relationship is a catalyst for academic research and a beacon of direction, alleviating the dullness of academic research.

Sincere thanks to Simone, when I appeared in front of you with my poor English, your care and patience relieved my anxiety at the beginning of my doctoral study, and your patient guidance gave me confidence when I had to face the first report.

I want to sincerely acknowledge the time and interest of the members of my defense committee: Prof. Dr. Olivia Merkel, Prof. Dr. Stefanie Fenske, Prof. Dr. Susanne Koch, and Prof. Dr. Franz Bracher. Thank you for accepting my invitation and spending your

time on reviewing on my thesis.

I am very grateful to Ling, the important partners who appeared in my doctoral career, who also fought side by side and accompanied each other, as well as the good-tempered, and kind friends Lucas and Pengyu, and Hong. They constituted a ray of sunshine during my doctoral study, helping me analyze and solving problems. It is even better to have your doctoral study accompanied by you.

Thanks to Jana, Julia, Maibritt, Patricia, Chriss and Amelie, in helping me with experimental techniques and my daily questions. I am very grateful to my collaborators Dietrich and Josef, they let me understand the meaning and importance of cooperation more comprehensively, and let me feel the pleasure of working together to solve scientific research problems. I am very grateful to all the friends I met in Munich for helping each other and overcoming difficulties together.

I would like to thank the China Scholarship Council for offering me the opportunity to study abroad and for the financial support that allows me to stay in Germany.

Finally, I am very grateful to my family who are far away in China and my lover. During my doctoral study, they have always been my strong backing and spiritual support, eliminating my worries and enhancing my confidence and motivation to complete my doctoral study. Especially my lover, who can always provide me with positive emotional value, and the discussion with him is also an important support for the development of my project, and he is not to mind taking the trouble; share joy, give me selfless love and support; we fight side by side, and hope we could gain together.

As I write this, I recall the bits and pieces of my doctoral study in my heart, and these bits and pieces will surely become my precious wealth in the future. A man should be independent at the age of thirty, and I will rush to my future with great gratitude and blessings.